

Gas Rich Dwarfs from the PSS-II

III. HI Profiles and Dynamical Masses

Jo Ann Eder

Arecibo Observatory, HC3 Box53995, Arecibo, PR 00612; eder@naic.edu¹

and

James M. Schombert

Department of Physics, University of Oregon, Eugene, OR 97403; js@abyss.uoregon.edu

ABSTRACT

We present Arecibo neutral hydrogen data on a sample of optically selected dwarf galaxies. The sample ranges in HI mass from $10^6 M_\odot$ to $5 \times 10^9 M_\odot$, with a mean of $7.9 \times 10^8 M_\odot$. Using estimated HI radii, the HI surface densities range from 0.6 to $20 M_\odot \text{ pc}^{-2}$, all well below the critical threshold for star formation (Kennicutt 1998). M_{HI}/L values of the LSB dwarfs range from 0.3 to 12 with a mean value of 2.0.

Dynamical masses, calculated from the HI profile widths, range from $10^8 M_\odot$ to $10^{11} M_\odot$. There is a strong correlation between optical luminosity and dynamical mass for LSB dwarfs implying that the dark matter (whether baryonic or non-baryonic) follows the detectable baryonic matter.

1. INTRODUCTION

The study of low surface brightness (LSB) galaxies presents an enormous observational challenge. LSB galaxies often too faint for more than limited optical study by broadband imaging. Spectroscopy and near-IR are practically impossible due to the fact that too few galaxy photons are emitted per square arcsec compared to the brightness of the night sky. Even a nominal number of HST orbits requires rebinning to obtain reliable S/N, which then loses the high resolution advantage of space imaging. However, one intrinsic characteristic has provided an avenue to study this class of galaxies, a majority of LSB galaxies contain copious amounts of neutral hydrogen (Schombert *et al.* 1992, Impey *et al.* 1996). This provides both a quick method to confirm the reality of objects, barely visible in the optical, while simultaneously providing their distance and crude kinematic information.

Dwarf galaxies are the most numerous class of galaxies in the Hubble sequence forming a large component of the number density of galaxies. For example, over 80% of the Local Group are classed as dwarfs and their space densities are higher even in cluster environments. They are found in all types of environments, from dense clusters to the field. They span the range of morphological types, from elliptical to highly irregular. And they cover a full range of current star formation rates, from quiescent dE's to intense BCD's (Sandage and Binggeli 1984). Although dwarf galaxies are low in metallicity (Skillman and Kennicutt 1993), they are by no means zero-metallicity protogalaxies. And, while dwarf galaxies are interesting for their internal properties and star formation histories, they also serve as probes to the characteristics of dark matter (Ashman 1992) and are tracers of large scale structure (Eder *et al.* 1989, Zwaan *et al.* 1995).

¹The Arecibo Observatory is part of the National Astronomy and Ionosphere Center which is operated by Cornell University under contract with the National Science Foundation.

Despite numerous studies on cluster and field dwarfs, it is still unclear whether dwarf galaxies are a continuation of the spiral sequence or whether they form a distinct population, possibly fossil remnants from the era of galaxy formation. Information about the gas content of dwarf galaxies is therefore critical to an understanding of their place in the hierarchy of galaxies. Unfortunately, our knowledge of the properties of dwarf irregulars is hampered by small catalogs because of difficulty in detecting them due to their LSB nature and small angular size. In order to improve the sample of dwarf irregular galaxies available for study, we have identified a new sample of 458 candidate dwarfs from inspection of 49 fields of the new Palomar Sky Survey (PSS-II) directed towards the North and South Galactic Caps. Previous papers have presented the catalog and the optical data (Eder *et al.* 1989, Schombert, Pildis, and Eder 1997, Pildis, Schombert and Eder 1997). This paper presents the single-dish Arecibo 21 cm data for this sample and determines the dynamical mass for dwarfs with optical measurements. The impact of these parameters on the star formation history of LSB dwarfs is explored in a latter paper (Schombert, McGaugh and Eder 2000).

2. OBSERVATIONS

In this paper, we report on the 21 cm observations of three samples of dwarf galaxy candidates selected visually from photographic plates of the Second Palomar Sky Survey (PSS-II). All of the samples were chosen so as to optimize their observation with the Arecibo radio telescope, meaning they lie between -5 and $+35$ in declination. The first sample (Sample 1) of 178 candidates was obtained from 15 fields located on regions of the fall sky occupied by a nearby void. The plates used were high quality preproduction plates. Of these candidates, 132 were observed at 21 cm. The void is centered at RA = 0h45m, Dec = $+20$, $v = 3500$ km sec^{-1} , and is of roughly spherical shape with a diameter of 1500 km sec^{-1} . The second sample (Sample 2) of 278 was identified using methods similar to those for the first sample from 35 random fields between RA's of 7h to 16h and Dec's of 10 to 25, irrespective of galaxy density. Of these, all were observed at 21 cm. The third much smaller sample of 27 (Sample 3) consisted of new dwarf candidates identified from a visual reexamination of one of the fields of Sample 1 (Field 409), using the final PSS-II production plates. Sample 3 also included observations of some of the dwarf candidates from Sample 1 which were not originally observed with 21 cm due to a lack of telescope time.

All objects on the plates with angular diameters greater than 20 arcsecs, irregular appearance (Sm, Im, Irr, dI) and low surface brightness were selected. Low mass implies instability, at least with respect to the pattern of star formation. Thus, irregular structure is nominally associated with dwarf galaxies (unless the star formation is completed, as in a dwarf elliptical). Basically, late-type galaxies can be broken down into three morphological types; those with bulges and LSB disks (Sc and Sd class, those with apparent axial symmetry but no bulges (Sm class) and those with no symmetry (Im class). However, morphology is only weakly related to the mass of a galaxy. There are many irregular galaxies that are massive (Hunter and Gallagher 1986) and many spirals which are dwarf-like in luminosity and size (Schombert *et al.* 1995). In addition, many high luminosity events, such as galaxy-galaxy interactions, are also associated with irregular morphology, although usually of a nature that identifies them as tidal in origin. Irregular morphology, by itself, is not a sufficient criteria for dwarf classification, but is sufficient for the development of a candidate list. The coordinates of each candidate dwarf were taken directly from the plate material using a fine ruler and the position of SAO stars. Accuracy of the coordinates were typically ± 15 arcsecs based on the centering of CCD imaging, which is sufficient for detection with the Arecibo beam of 3 arcmin diameter. Further details of the selection of the three samples can be found in our previous papers: Eder *et al.* 1989 (Sample 1) and Schombert, Pildis, and Eder 1997 (Samples 2 and 3).

Follow-up CCD images in V and I for most of those galaxies detected in H I from Sample 2 were obtained on the Hiltner 2.4m telescope located at Michigan-Dartmouth-M.I.T. (MDM) Observatory. We obtained images using either a Thomson 400×576 pixel CCD ($0.25 \text{ arcsec pixel}^{-1}$) or a Ford-Loral 2048×2048 pixel CCD binned 3×3 ($0.51 \text{ arcsec pixel}^{-1}$), with minimal exposure times of 25 minutes in Johnson V and 15 minutes in Johnson I. Analysis of these images reveal that the candidates are gas-rich dwarf galaxies with total luminosities of $M_V > -18$ mags, central surface brightnesses between 21 and 23 I mags arcsec^{-2} , exponential scale lengths of typically less than 3 kpc and mean isophotal diameters (of approximately the Holmberg diameter) of 8 kpc (as compared with a mean of 30 kpc for the UGC galaxies, Pildis, Schombert and Eder 1997). A sample of comparable size to ours would be the Virgo Cluster dwarfs (Hoffman *et al.* 1997) but these dwarfs reside in a cluster environment while ours inhabit a range of environmental densities.

We observed the dwarf candidates for the HI line at 21 cm with the Arecibo 305m telescope during the 1988, 1992 and 1993 observing season. All observations were made with the 21 cm dual-circular feed positioned to provide a maximum gain (8 K Jy^{-1}) at 1400 MHz. The 2048 channel autocorrelator was used and the independent, opposite polarized signals were each divided into two subcorrelators of 512 channels. In order to search a larger velocity space, the secondary local oscillators of each polarization set of subcorrelators were offset on either side of the standard local oscillator frequency of 260 MHz by 8.75 MHz, allowing a total velocity coverage of 8000 km sec^{-1} , a velocity resolution of 8.6 km sec^{-1} , and some overlap at the band edges. The observations were centered on 4000 km sec^{-1} , which avoided detection of the strong Galactic hydrogen signal on the low-velocity end, and extended to 8120 km sec^{-1} . Observations were made in the total power mode with 5 minute ON- source and OFF-source observations. In most cases, only one 5-minute ON-source integration was required for detection. Wherever possible, the zenith angle was kept less than 14 degrees to minimize the degradation of the gain.

Efforts were made to assure that the signal was due to the candidate galaxy. The field of each position was examined on the original plates and also with NED to check for possible sources of confusion. Because many of the detections were very narrow, the possibility existed that they were actually caused by radio frequency interference (RFI). However, RFI confusion can be distinguished by their polarization properties and/or, with 3-level sampling, by the ringing they cause in the band which is eliminated with hanning smoothing. Those narrow detections that were still suspicious were reobserved to confirm their authenticity. Higher resolution observations of several narrow line detections revealed double-horned features.

3. ANALYSIS

3.1. Galaxy Data

All three samples were analyzed and reduced in the same fashion. Calibration of the spectra for atmospheric correction and noise diode variation with frequency was performed during the phase of translation into export format for compatibility with the Arecibo Observatory ANALYZ-GALPAC analysis system. Baseline fitting, removal, and parameter extraction were all performed using the latter package. The width, referred to hereafter as W_{50} , is defined as the full width across the profile measured at a level of 50% of the peak flux.

In Table 1 we present the results of the analysis for the 250 galaxies whose digital spectra have been examined. In addition, 143 galaxies which were searched for, but not detected, are also listed in Table 1. The nominal search range was 1000 to $8,000 \text{ km sec}^{-1}$, with occasional extensions to $12,000 \text{ km sec}^{-1}$. The typical RMS values were 3 mJy. All distance related values in this paper use values of $H_o = 75 \text{ km sec}^{-1}$

Mpc⁻¹. All the data included in this paper can also be found in ASCII format at zebu.uoregon.edu/~js.

Details of the entries in Table 1 are as follows:

- Column (1): Object ID, based on the PSS-II field number and a running number for the dwarfs found on that field.
- Columns (2) and (3): Right ascension and declination in the 1950.0 epoch. These are measured off the PSS-II plates themselves and are accurate to 15 arcsecs.
- Column (4): The heliocentric velocity, V_h of the HI line, taken at the midpoint of the profile (50% of peak level).
- Column (5): The velocity corrected for the motion of the Sun relative to the center of mass of the Local Group, according to the precepts of de Vaucouleurs, de Vaucouleurs, and Corwin (1976), V_o , in km sec⁻¹.
- Column (6): The velocity width, W_{50} , in km sec⁻¹. No corrections have been made for inclination or turbulent broadening.
- Column (7): The profile shape where S means single-horned and D means double-horned. A semi-colon indicates uncertain classification.
- Column (8): The observed integrated 21-cm HI line flux, $S = \int S_V dV$ in Jy km sec⁻¹.
- Column (9): The HI gas mass of the object, in M_\odot , calculated using the standard conversion from flux to gas mass.
- Column (10): Observing run number from which the data was taken, where run #1 is Sample 1 observed in 1986, #2 is Sample 2 and #3 is Sample 3, both observed in 1992 and 1993.

3.2. Notes on Individual Galaxies

409-4,476-5 – Velocity scale in the spectrum is not correct because the LO synthesizer was set incorrectly. The velocities in the Table are the correct values.

409-7 – 1.5 arcmin from SRGb 062.12 ($v=7333$ km sec⁻¹)

409-11 – 8.5 arcmin from 409-10

409-16 – 6.1 arcmin from N7773 ($v=8486$ km sec⁻¹)

409-17 – 3.0 arcmin from KUG 2356+303

409-18 – 1.6 arcmin from U152 ($v=4863$ km sec⁻¹)

474-9 – 8.1 arcmin from N304 ($v=4991$ km sec⁻¹)

476-2 – also U948

476-4 – also U1073

476-5 – also U1084

495-1 – 5.8 arcmin from U4361 ($v=3741 \text{ km sec}^{-1}$)

495-3 – detected as F495-V1 (LSB2)

508-1 – The dwarf HI signal could be embedded in that of NGC 4961, detected here off center, but is buried in flux from primary galaxy. NGC 4961 detected by Shostak. The velocities and widths listed in the Table are measured at 50% of the mean flux

508-2 – near A1656

512-1 – lots of RFI

512-4 – 8.8 arcmin from KUG 1430+264

512-5 – observed in velocity range 0 - 12,000 km sec^{-1}

512-10 – 6.5 arcmin from IC4475

514-2 – observed in velocity range 0 - 12,000 km sec^{-1}

514-3 – paired with 514-4

514-5 – The spectrum is missing from the Figure

514-6 – observed in velocity range 0 - 12,000 km sec^{-1}

516-1 – observed in velocity range 0 - 12,000 km sec^{-1}

538-1 – 4.9 arcmin from U3 ($v=7882 \text{ km sec}^{-1}$)

538-2 – 7.8 arcmin from N7817 ($v=2309 \text{ km sec}^{-1}$)

538-15 – also U12843

538-16 – also U12846

538-18 – 8.3 arcmin from U12916 ($v=6352 \text{ km sec}^{-1}$)

539-2 – also U159

539-5 – also IC1542

539-6 – also U200

540-2 – 7.9 near U425 ($v=5841 \text{ km sec}^{-1}$)

540-3 – also U477

540-8 – 1.3 arcmin from F474-10

559-3 – Malin object, 9.3 arcmin from U3920

563-2 – detected as F563-V2 (LSB2)

563-3 – 7.7 arcmin from U4588 ($v=4264 \text{ km sec}^{-1}$), detected as F563-V1 (LSB2)

563-4 – dwarf spiral, detected as F563-1 (LSB1)

564-2 – measured parameters are uncertain because of overlapping RFI

564-8 – detected as F564-V3 (LSB2)

564-12 – 7.4 arcmin from U4729 ($v=3900 \text{ km sec}^{-1}$)

564-15 – dwarf spiral

565-2 – UGC 5005, detected by Bicay and Giovanelli

565-3 – possibly two merged signals - several nearby galaxies are within 1 arcmin on the CCD field

565-5 – signal is blend of UGC 5086 and NGC 2903 in the beam and sidelobes

565-10 – KARA 68-056, not detected as F565-V4 (LSB2)

568-3 – REIZ 363, 3.4 arcmin from U5629 ($v=1236 \text{ km sec}^{-1}$)

568-4 – ZWG 094.005

568-5 – observed in velocity range 0 - 12,000 km sec^{-1} but had strong RFI (rms=2.3mJy)

570-3 – detected as F570-V1 (LSB2)

570-4 – detected as F570-7 (LSB2), 4.5 arcmin from IC2703

570-6 – poor S/N, companion to D571-5

571-3 – 8.7 arcmin from AGC210538 ($v=6196 \text{ km sec}^{-1}$)

571-5 – two galaxy signals appear in the spectrum, due to two galaxies within 20 arcsec on the CCD image. The parameters listed in the table are from the face-on diffuse dwarf galaxy. The other signal is double peaked and therefore emanates from the inclined spiral ($v=5985 \text{ km sec}^{-1}$, $W=86 \text{ km sec}^{-1}$, $FI = 157.2 \text{ mJy km sec}^{-1}$)

571-6 – also not detected as F571-10 (LSB2)

572-5 – 8.3 arcmin from U6770

575-1 – I3840, detected as F575-2 (LSB2)

575-2 – UGC 8011

575-3 – I4107

575-4 – pair to 575-3

575-5 – KARA 68.215, in same beam as F575-3 detected in LSB2. The velocities and widths listed in the Table are measured at 50% of the mean flux

576-2 – strong continuum

576-6 – ZWG 101.005

576-7 – measured parameters uncertain because of interference

576-11 – MCG +03-34-034, 2.7 arcmin from U8448 ($v=7151 \text{ km sec}^{-1}$), probably U8448 off band

577-5 – dwarf spiral

577-6 – measured parameters uncertain because the galaxy spectrum is near the edge of the band, companion to D648-4

582-1 – probably off-beam detection of F582-2 (LSB2)

- 582-4 – 9.5 arcmin from F583-2
- 584-2 – also U10140, 6.1 arcmin from U411A ($v=2525 \text{ km sec}^{-1}$)
- 609-2 – also U385
- 609-3 – companion to D609-2
- 609-4 – UGC 472, detected by Bothun *et al.* 1985
- 609-5 – also U560
- 611-5 – detected as F611-1 (LSB2)
- 611-6 – also U883
- 611-7 – also U891
- 611-11 – 6.1 arcmin from F611-V2
- 611-13 – also U1026
- 611-14 – also U1056
- 611-18 – 8.7 arcmin from U1087 ($v=4485 \text{ km sec}^{-1}$)
- 631-3 – questionable signal at $v=168 \text{ km sec}^{-1}$, $W=33$, $FI=123 \text{ mJy km sec}^{-1}$
- 631-4 – questionable signal at $v=352 \text{ km sec}^{-1}$, $W=50$, $FI=147 \text{ mJy km sec}^{-1}$ 631-7 UGC 4115, detected by Bica and Giovanelli
- 631-7 – also U4115
- 631-8 – dwarf spiral
- 631-9 – questionable signal at $v=2280 \text{ km sec}^{-1}$, $W=59$, $FI=178 \text{ mJy km sec}^{-1}$
- 631-11 – questionable signal at $v=6130 \text{ km sec}^{-1}$, $W=60$, $FI=123 \text{ mJy km sec}^{-1}$
- 637-1 – very noisy spectrum
- 637-5 – 7.8 arcmin from IC581
- 637-7 – 7.5 arcmin from U5342 ($v=4560 \text{ km sec}^{-1}$) (pair?)
- 637-10 – observed in velocity range 0 - 12,000 km sec^{-1}
- 637-21 – observed in velocity range 0 - 12,000 km sec^{-1}
- 640-2 – 640-2,3 and 4 are all in the same beam (UGC 6006, UGC 6007). Signal is due to U6006 also detected by Schneider *et al.*
- 640-7 – UGC 5948, detected by Schneider *et al.*
- 640-8 – near NGC 3489
- 640-10 – UGC 5944
- 640-11 – measured parameters uncertain due to overlapping RFI, 5.4 arcmin from N3412 ($v=865 \text{ km sec}^{-1}$)

640-14 – near ZWG 066.072

640-15 – NGC 3559, detected by Bica and Giovanelli

646-4 – Rea 66

646-5 – 646-6 is also in the beam, signal could be from either one

646-7 – UGC 8091, detected by Lewis, Helou, and Salpeter

646-11 – UGC 8061 - detected by Schneider *et al.*

648-1 – solar interference

648-2 – very bad baseline and noise

648-4 – companion to D577-6

648-6 – solar interference

651-6 – comp to ZWG 076.018

656-1 – U10398 - detected by Schneider *et al.*

656-2 – U10281 - detected by Schneider *et al.*

656-4 – observed in velocity range 0 - 12,000 km sec⁻¹

656-5 – 9.2 arcmin from U10218 (v=1080 km sec⁻¹)

685-6 – also U1323

685-18 – also U1515

685-19 – remeasured parameters since Eder *et al.* , 4.4 arcmin from IC1772

709-5 – KARA 68.060

709-7 – 9.5 arcmin from N3130 (v=8206 km sec⁻¹)

709-9 – 9.2 arcmin from U5304 (v=12308 km sec⁻¹)

709-10 – 5.3 arcmin from U5304 (v=12308 km sec⁻¹)

721-1 – ZWG074.037 also in beam

721-5 – dwarf spiral, detected as F721-V4 (LSB2)

721-7 – 4.1 arcmin from N5463 (v=7235 km sec⁻¹) (pair)

721-8 – companion to D721-9

721-10 – limits of the measured galaxy spectrum are uncertain

721-14 – signal is from U8995 at 140219+090224 detected by Bothun *et al.* 1985

721-15 – broad wings - parameters uncertain - NGC 5511 interaction

723-3 – signal on edge of spectrum, parameters uncertain

723-4 – 6.3 arcmin from U9356 (v=2225 km sec⁻¹)

723-9 – also U9500

749-3 – also U12416

749-6 – also U12480

749-7 – 5.9 arcmin from N7587 ($v=8917 \text{ km sec}^{-1}$)

749-8 – 5.0 arcmin from N7593 ($v=4108 \text{ km sec}^{-1}$)

749-9 – 5.8 arcmin from U12497 ($v=3761 \text{ km sec}^{-1}$)

749-10 – also U12497

749-12 – also U12553

749-14 – also U12562, 8.2 arcmin from N7641 ($v=7872 \text{ km sec}^{-1}$)

749-17 – 8.4 arcmin from U12687 ($v=6158 \text{ km sec}^{-1}$)

774-1 – dwarf spiral

774-4 – PK 215+11.1

822-4 – remeasured parameters since Eder *et al.* , 3.7 arcmin from D822-5

822-6 – also F750-2

822-14 – 8.8 arcmin from N7757 ($v=2956 \text{ km sec}^{-1}$) (pair)

3.3. Mass Estimates

To determine the dynamical masses from the HI profiles, inclinations and metric sizes are needed. To this end, CCD images were obtained for 116 galaxies at the 2.4m MDM telescope. The isophotometric ellipse fitting was done as described in Pildis, Schombert and Eder 1997. Scale lengths were derived from least-squares fitting of an exponential function to the data in the surface brightness-radius plane.

Due to their LSB nature, the inclination measurements of dwarf galaxies are problematic (Tully *et al.* 1978, Lo *et al.* 1993). Since HI rotation velocities are being used, strictly speaking HI diameters should also be used. However, numerous studies have shown that the HI surface densities follow the optical surface densities (see McGaugh 1992). Thus, we adopt the optical parameters for inclination as based on the eccentricity of the ellipse at the 25 mag arcsec⁻² isophote. The R_{25} isophotal radius, axial ratio and I magnitude are listed in Table 2.

The dynamical mass is determined from the virial theorem using the prescription of Staveley-Smith, Davies and Kinman (1992, hereafter SDK). However, to complicate matters, ellipticity studies indicate that dwarf galaxies are primarily triaxial with particular signatures in their structural parameters that confirm their non-oblate nature (Schombert, McGaugh and Eder 2000). If dwarf galaxies are not oblate rotators, then as discussed in SDK, the use of a pure rotation term to calculate the dynamical mass will underestimate this value by as much as 30%. Hence, we adopt SDK’s virial mass estimate, M_{dyn} , as given by

$$M_{dyn} = 2.3 \times 10^5 (V_{rot}^2 + 3\sigma^2) R_{HI}$$

where V_{rot} is the rotation velocity, σ is the isotropic velocity dispersion and R_{HI} is the outer radius of the HI emission. The velocity dispersion is assumed to be 10 km sec^{-1} , the standard value for late-type galaxies (Shostak and van der Kruit 1984). High resolution HI maps of gas-rich dwarf galaxies also indicate a typical velocity dispersion of 10 km sec^{-1} (Skillman *et al.* 1988, Lo *et al.* 1993). Note that, for dwarfs without rotation, V_{rot} could be replaced with σ and the dynamical masses is underestimated by a factor of 3, but we have assumed rotation in our discussion.

We calculate V_{rot} from the measured HI profile width, correcting for inclination and velocity dispersion such that

$$W_{50} = 2(V_{rot}\sin i + 1.18\sigma)$$

where the inclination, i , is determined from the axial ratio of the outer isophotes of the dwarf galaxy. The remaining variable is R_{HI} , the radius of the edge of the HI emission. We can measure R_{25} , the radius of the $25 \text{ B mag arcsec}^{-2}$ isophote directly from the optical images. HI mapping studies indicate that the HI diameter of dwarf galaxies is much larger than the optical radius. Van Zee, Skillman and Salzer (1998) found that the HI diameter is approximately 4 times the optical radius for a mapping study of 5 dwarfs. However, these dwarfs were selected as having an overabundance of HI. Salpeter and Hoffman (1996) discovered a correlation between optical and HI radius, such that $R_{HI} = 2.3R_{opt}^{-0.11}$ for a sample of 109 dwarf irregular galaxies. Based on this evidence, we have set $R_{HI} = 2.3R_{25}$ for the dwarf sample and determined all scale length values based on this conversion. The calculated values M_{dyn} are listed in Table 2 along with the ratio of M_{HI}/M_{dyn} .

4. DISCUSSION

4.1. What is a dwarf galaxy?

Our understanding of dwarf galaxies, their properties, contents and star formation histories, has changed sharply, mostly because our catalogs of dwarf galaxies have expanded in the last decade. Our initial view of dwarf galaxies were based on our studies of the LMC, SMC and other Irr class galaxies in the Local Group (Holmberg 1957) and low luminosity dwarf spheriodals such as Leo A. These objects, although interesting in their own right, do not properly represent the range in mass, appearance and star formation history that define what we consider today to be the class of dwarf galaxies. For example, in the late 1950's, de Vaucouleurs (1959) extended the late-type Hubble classes into the Sd, Sm and Im types to delineate the gradual loss of spiral structure. Most of these extreme late-type galaxies would later be defined as dwarfs based on their optical magnitudes (see Sandage and Binggeli 1984); however, they do not define the dwarf galaxy population.

Inspection of nearby clusters (Virgo and Fornax) revealed an extensive population of gas-poor elliptical dwarfs and gas-rich irregular dwarfs, subsequently called dE and dI to indicate their morphological link to ordinary ellipticals and irregulars. The similarities between the dwarf ellipticals and irregulars to their giant counterparts (such as mass-metallicity relations, fundamental plane parameters and star formation) did appear to simplify the Hubble sequence as one divided by morphological class on one axis and by luminosity (and therefore mass) on the other. However, later work on field dwarfs (Eder *et al.* 1989, Schombert *et al.* 1997) showed that there is very little difference between the cluster dI class and the de Vaucouleurs Im class.

With the addition of a wide variety of morphological types, the definition of a dwarf galaxy has become blurred in the last decade. If asked, a theorist would define a dwarf galaxy by mass, then consider various formation scenarios that produce a mass spectrum. Unfortunately, dark matter becomes fractionally more significant in galaxies with decreasing mass (Ashman 1992), and this means that galaxy mass does not map, in a direct fashion, into observables such as luminosity, size or even rotational velocity. In addition, to make a difficult situation even worse, lower luminosity, density and size make the necessary observables laborious or impossible to obtain with our current technology and/or limited telescope time.

Within the observables, there are several methods in which to define a dwarf galaxy. For example, one can define a dwarf galaxy by optical luminosity (Tammann 1980). Since a galaxy’s optical luminosity is the primarily due to the photons emitted by stellar photospheres, then the total luminosity should reflect the stellar mass. With a stable IMF, the connection between luminosity and mass is parameterized by $\Upsilon_* = M_*/L$, the stellar mass, M_* divided by the total luminosity of a galaxy, L . Therefore, a dwarf galaxy could be defined by some boundary in optical luminosity as it reflects into stellar mass. However, since the fraction of dark matter (baryonic and non-baryonic) increases with later type galaxies (Ashman 1992), the use of luminosity to trace mass begins to decouple or has too many variables.

Dwarf galaxies are typically low in density, so division by central surface brightness (based on fits to the galaxy’s profile) can be used as an indicator of dwarfness. There is some physical reasoning to support the idea that all LSB galaxies should be dwarf systems. To produce low stellar densities would require very low past star formation rates and, hence, low total stellar mass and luminosity. Low surface brightness does not necessarily mean low stellar densities, but the colors of LSB galaxies rule out any highly unusual Υ_* (McGaugh and de Blok 1997) implying that low optical density is indeed low stellar density. Or, conversely, we might expect a dwarf galaxy of low mass to have low mean density which, in turn, inhibits star formation to produce a LSB object. One could argue that initial conditions, such as the amplitude of the density perturbation in the early Universe from which the galaxy will form, produces a necessary connection between a dwarf galaxy and a LSB galaxy. Unfortunately, the discovery of large Malin galaxies destroyed the notion that all LSB galaxies are dwarfs. In fact, most LSB disk systems are comparable in size to the ordinary spirals that make up the Hubble sequence (McGaugh, Schombert and Bothun 1995).

Low mass implies instability, at least with respect to the pattern of star formation. So, irregular structure is nominally associated with dwarf galaxies (unless the star formation is completed, as in a dwarf elliptical). Basically, late-type galaxies can be broken down into three morphological types; those with bulges and LSB disks (Sc and Sd class, those with apparent axial symmetry but no bulges (Sm class) and those with no symmetry (Im class). However, morphology is only weakly related to the mass of a galaxy. There are many irregular galaxies that are massive (Hunter and Gallagher 1986) and many spirals which are dwarf-like in luminosity and size (Schombert *et al.* 1995). In addition, many high luminosity events, such as galaxy-galaxy interactions, are also associated with irregular morphology, although usually of a nature that identifies them as tidal in origin. Irregular morphology, by itself, is not a sufficient criteria for dwarf classification.

The most promising approach is to use the size of a galaxy as a measure of its dwarfness. A combination of angular size and irregular morphology were the criteria used in the initial construction of the PSS-II LSB dwarf catalog. Our previous LSB surveys (Schombert and Bothun 1988) was rich in LSB disks with scale lengths greater than 4 kpc, but few dwarf galaxies. That survey used a minimal angular size of one arcmin, the same as the UGC, to determine the bias against LSB galaxies in our catalogs. This PSS-II LSB dwarf survey set the criteria to be between 30 arcsecs and one arcmin, with a dramatically different metric size distribution as seen in Figure 3 of Schombert *et al.* (1997). With the acquisition of surface photometry and a H I redshift, a proper comparison of scale length sizes for the sample can be made (shown in the top panel

of Figure 3). Most of the objects (90% of the sample) turn out to be quite small, less than the typical disk galaxy (3.2 kpc, de Jong 1996), testifying to the power of using morphology to select dwarf galaxies. We suspect that many of the undetected dwarf-like objects are probably background Sc’s outside the velocity range of the observing set-up for the Arecibo telescope. We conclude from Figure 3 that a robust method of collecting a sample of dwarf galaxies is to select objects by irregular morphology over a limited angular size (in our case, 30 to 60 arcsecs).

4.2. HI Profiles

A sample of 458 candidates were found by visual inspection of the PSS-II plates. Each candidate object was assigned a quality index as a measure of its probability to be a dwarf galaxy based on its morphological appearance. This is a purely subjective system, based on an objects irregular shape, lack of coherent spiral patterns, small to non-existent H II regions and a general LSB appearance. Most of these galaxies would be classified as extreme late-type (Sm, Im, Irr or dI) and a more complete discussion of their morphological and properties can be found in Schombert, McGaugh and Eder (2000). From our initial sample, 432 with high quality indices were observed on the Arecibo 300m telescope at 21-cm out to a velocity of 8,000 km sec⁻¹.

Of the 432 galaxies observed, 259 (60%) were detected. The objects not detected are probably background LSB spirals (with spiral patterns that were not visible on the plates), gas-poor dwarfs (dE’s) or dwarfs whose HI masses and distance fall below the sensitive limit of the telescope. A small sample of the nondetections were reobserved in a velocity range of 4,000 to 12,000 km sec⁻¹ in order to determine how many of the nondetected candidates were actually distant spiral galaxies. Of 18 candidates, 10 were detected at the higher velocities. However, only 4 of these have velocity widths which suggest a normal spiral galaxy (one being the Malin object D559-3 with a velocity width of 576 km sec⁻¹). The loss of gas-poor dwarfs from the sample is unfortunate since the distribution of dE’s, outside of a cluster environment, is not known. In fact, the existence of a true dE, independent of a high local density or nearby companion, has not been confirmed (Binggeli, Tarenghi and Sandage 1990).

The spectra of all the detections from the three samples are presented in Figure 1. A hanning smoothing function has been applied, followed by a boxcar of 3. Each panel displays the raw data as well as the fitted baselines. A majority of the sample requires only a 2nd or 3rd order polynomial to flatten the baseline. As seen by other studies, most dwarfs have the classic double-horned profile indicative of rotation, although the data is too low in resolution to discern features such as asymmetries, filled-in cores or extended line wings (Hoffman *et al.* 1996, Matthews, van Driel and Gallagher 1998, Staveley-Smith, Davies and Kinman 1992). Skewed profiles may be due to confusion with nearby sources or pointing errors.

The HI profiles can be divided into two types, gaussian and double-horned. A galaxy with a flat or rising rotation curve, and a distribution of gas that declines with radius in the form of a power law, will exhibit a HI profile that has two peaks with a flat plateau region between them (see Giovanelli and Haynes 1988). The 246 spectra in Figure 1 were classified as either double horned, single horned or uncertain (listed in Table 1). Double horned profiles (such as D475-4 or D704-2) have distinguishable peaks or a plateau shape. Single horned profiles display a smooth gaussian shape with no indication of flattening. In many cases (e.g. D709-5), the profile is broad, but the double horn shape is unclear due to noise. In other cases (e.g. D702-1), there is an asymmetry that distorts the profile. Profiles with noisy plateaus are classed as uncertain. For the 246 spectra, 140 are double horned, 61 are single horned and 45 are uncertain. Assuming the uncertain profiles are evenly divided between single and double (most are broad and probably double

horned), then double horned profiles are found in at least 70% of the sample.

The distribution of HI fluxes and HI profile widths are shown in Figure 2. All the detections are well above the 3σ level given the mean fluxes and velocity widths. The mean velocity width, even without inclination corrections, is low compared to a typical late-type galaxy sample (see Schombert, Pildis and Eder 1997) confirming our intent to acquire a sample of low mass objects. A handful of objects with $W_{50} > 150$ km sec $^{-1}$ represent a few Malin type objects, irregular in their morphology, that mimic a dwarf galaxy’s appearance yet are actually large, distant spirals.

The metric scale length (α) distribution, discussed in §4.1, is shown in the top panel of Figure 3. Based on exponential fits to the I band surface brightness profiles, α provides the most fundamental property of a galaxy, its characteristic size. While the isophotal size of a galaxy, combined with its mean surface brightness, determines its visibility and detection probability. The typical scale length for a disk galaxy is indicated.

The redshift distribution of the detected dwarfs is shown in the bottom panel of Figure 3. The spatial distribution was shown in Figure 6 of Schombert, Pildis and Eder (1997). To repeat that paper’s conclusion, LSB dwarfs trace the same large scale structure as brighter galaxies. Figure 3 confirms that a majority of the dwarfs are located between 2000 and 6000 km sec $^{-1}$, although there is a strong mass dependence. This dependence on mass is shown in the lower panel of the Figure 3 as a plot of HI mass versus redshift. The solid line shows the telescope 3σ detection limit for a dwarf galaxy with a line width (W_{50}) of 75 km sec $^{-1}$. A majority of the detections lie above this line. Objects below the limit all have line widths smaller than the assumed 75 km sec $^{-1}$ and, thus, a higher S/N per channel. Note that the lowest mass object ($M_{HI} = 2.5 \times 10^5 M_{\odot}$) is located at less than 500 km sec $^{-1}$. This plot demonstrates that the search for very low mass HI-rich galaxies is extremely difficult as a combination of confusion with Galactic HI emission and small angular size makes their inclusion in any catalog problematic (see Schneider and Schombert 1999). It is also apparent from Figure 3 that a search for objects with $M_{HI} < 10^7 M_{\odot}$ will require a smaller angular limit in order to catalog candidates and deeper HI observations to obtain sufficient S/N (see also Zwaan *et al.* 1997) and that contrary to expectations (Briggs 1997) our galaxy catalogs are incomplete even in the local region of the Universe.

4.3. HI Masses and M_{HI}/L

The distribution of HI masses, calculated using the standard formula of distance and HI flux (Giovanelli and Haynes 1988) is shown in the top panel of Figure 4. The sample has a mean value of $M_{HI} = 7.9 \times 10^8 M_{\odot}$ and a sharp cutoff at $M_{HI} = 4.0 \times 10^9 M_{\odot}$. This can be compared to the UGC HI sample (see Figure 4, Schombert, Pildis and Eder 1997) where the mean HI mass of a UGC selected galaxy is $M_{HI} = 3.0 \times 10^9 M_{\odot}$. Figure 4 shows that, whereas LSB galaxies are gas-rich, this does not mean that LSB dwarfs have high gas masses. The distribution of HI masses for this sample still defines the low-end of a gas mass distribution from any galaxy catalog and a galaxy selected to be dwarf-like by HI mass is as valid as classification by total mass or luminosity.

The bottom panel of Figure 4 displays mean HI surface density (Σ_{HI}) for each dwarf with available optical imaging. The HI radius has been used to determine the average surface density (assuming the same axial ratio as the outer optical isophote). The Σ_{HI} values range from 0.6 to 20 M_{\odot} pc $^{-2}$ with a mean value of 5. The importance of Σ_{HI} to star formation was outlined in Kennicutt (1989) where he found that star formation follows a power-law in ordinary galaxies (the so-called Schmidt law, $SFR \propto \Sigma_{HI}^{\alpha}$). Key

to Kennicutt’s findings was that there exists a threshold for star formation based on the Toomre (1964) instability criterion, the balance between gravity and rotation/thermal pressures. In a study of five dwarf galaxies, van Zee *et al.* (1997) found that the critical threshold was between 9×10^{20} and 6×10^{21} atoms cm^{-2} , which corresponds to the range of 5 and 30 $M_{\odot} \text{pc}^{-2}$ in HI mass after corrections for neutral helium and other metals. This indicates that the mean HI surface densities for most of the LSB dwarfs in this sample are below the critical threshold density for star formation. Of course, there can exist local density enhancements that could form sites of star formation. However, the average surface density for the galaxy is below the threshold and this would explain the LSB nature to the dwarf sample, where star formation has occurred in the past (since there is some measurable stellar luminosity), but that this star formation has been inhibited and the current star formation levels are very low (McGaugh and de Blok 1997).

The fraction of a galaxy’s mass in the form of gas increases with later Hubble types and can dominate the kinematics of a dwarf galaxy (Meurer *et al.* 1996). In addition, the amount of gas in dwarf galaxies increases with decreasing surface brightness to the point where many of these dwarfs have gas fractions between 0.7 and 0.9 whereas the typical spiral have $f_g \approx 0.4$ (Schombert, McGaugh and Eder 2000). Thus, the Hubble sequence can be described as a declining ratio of stellar to gaseous material, where early-type galaxies are dominated by stars, later types by gas. This ratio is typically expressed as M_{HI}/L and is shown in Figure 5 plotted against galaxy central surface brightness (μ_o) and galaxy color ($V - I$). The LSB dwarfs have a much higher value of M_{HI}/L than the ordinary spirals, taken from the de Jong (1996). The distribution of M_{HI}/L herein is similar to that of van Zee, Haynes and Giovanelli (1995), a study of extreme M_{HI}/L galaxies from the Haynes and Giovanelli HI survey with the M_{HI}/L values ranging from 0.3 to 12 and a mean value of 2.0. This average M_{HI}/L found here is the same as the value found by van Zee, Haynes and Giovanelli (after adjustment for the I band luminosities) and we also find very few galaxies with $M_{HI}/L > 10$ even though this sample was selected by optical morphology rather than M_{HI}/L ratio.

By itself, the HI properties of LSB dwarfs are poorly correlated with optical surface brightness or color. But, when compared with the de Jong sample, it is clear that the dwarfs continue the trend of increasing M_{HI}/L with decreasing surface brightness and bluer colors. Both these correlations provide insight into the star formation history of dwarf galaxies. Higher M_{HI}/L ’s with lower central surface brightness reflects the obvious connection between a galaxy’s gas supply and the density of its stellar population. LSB dwarf galaxies have converted very little of their gas into stars (i.e. their past star formation has been inefficient and/or at a very low rate). Thus, they maintain a high gas mass value in comparison to an even lower luminosity.

The correlation with galaxy color follows from the surface brightness correlation. Though star formation in LSB galaxies occurs at a low rate (McGaugh 1992), even the smallest amount of star formation has a large impact on the total galaxy color due to the low surface brightness of the underlying population. Galaxies with highest M_{HI}/L values have the bluest $V - I$ colors, meaning that the portion of the stellar population that contributes a majority of the optical luminosity in a LSB dwarf galaxy is quite young (see also Schombert, McGaugh and Eder 2000).

4.4. Dynamical Masses and Baryonic Matter

The dynamical mass values are listed in Table 2 for the dwarf galaxies with optical imaging and the histograms of M_{dyn} and M_{dyn}/L values are found in the of Figure 6. Note that this ratio is determined using I band luminosities. For the typical dwarf color of $B - I = 1.5$, the M_{dyn}/L values are a factor of 4 higher

than similar B values (Staveley-Smith, Davies and Kinman 1992). In general, the dynamical masses are a factor of 10 higher than the HI masses, but still much lower than a typical spiral sample (de Jong 1996). Again, as we have seen with indirect mass indicators (luminosity and size), galaxies selected by dwarf-like morphology define a low mass population. As shown in Figure 6, LSB dwarfs range in M_{dyn}/L from 1.5 to 50 with a mean of 20. For comparison, the mean M/L of spiral galaxy pairs is 40 at radii of 100 kpc (Honma 1999).

A comparison of dynamical mass to stellar mass (as represented by the total I band magnitude of the dwarf) is found in Figure 7. Magnitudes in the I band are preferred over other bandpasses because stellar population models (Worthey 1994) show that the stellar mass to luminosity ratio (M_*/L) vary with time and star formation rate as a function of wavelength, but is most stable in the far-red. The use of the I band observations minimizes these stellar populations effects due to its distance in wavelength from the region around the 4000Å break. Thus, I band measurements 1) provide a more accurate estimate of the stellar mass of a galaxy, 2) obtain a luminosity measure that vary little with recent star formation and 3) determine structural parameters (such as scale length) which are undistorted by recent star formation events.

Although there is a great deal of scatter in the M_T^I versus M_{dyn} diagram, the LSB dwarf sample defines a linear correlation with a constant M/L slope. Immediately obvious is that none of the dwarfs have their total masses composed solely of stars. Nor is the total mass explained by the sum of the stellar and gas masses (see below). In other words, LSB dwarfs are dark matter dominated. Interestingly, the linear correlation means that the dark matter follows the stellar light, even for this sample of extreme M/L objects. One could interpret this one-to-one correspondence to indicate that dark matter is baryonic (i.e. baryons follow baryons). However, it is equally probable that the dark matter component is non-baryonic and simply accretes baryon material in a fashion that is proportional to its own mass. Certainly, with the discovery of massive neutrinos (see Turner 1997), it is now known that at least some fraction of the dark matter component in galaxies is non-baryonic.

The remaining question, regarding the dynamical mass estimates, is how much of a dwarf galaxies mass is in the form of observable baryonic material. This question is answered, graphically, in Figure 8 where we plot the ratios of stellar mass to dynamical mass and gas mass to dynamical mass. The stellar mass is calculated assuming a M_*/L of 1.2, based on the optical colors of LSB galaxies (McGaugh and de Blok 1997). Again, the advantage of I band magnitudes is that this value is very insensitive to recent star formation, varying only 10% for the range of observed optical colors in LSB dwarfs. The gas mass is calculated from the HI mass and multiplying for a factor of 1.4 to account for helium and metals. There has been no observed CO emission in LSB galaxies (Schombert *et al.* 1990) and the current star formation signature by H α emission is weak. Thus, we take the amount of molecular and ionized gas to be negligible. Although there has been discussion of ionization by extragalactic UV (Corbelli and Salpeter 1993), none has been detected in LSB galaxies. The sum of the stellar and gas masses produces the mass in baryons ($M_{baryons}$) for each galaxy shown in Figure 8.

Unlike the rest of the Hubble sequence, LSB dwarfs tend to have equal amounts of mass in the form of stars and gas. However, both these components are a small fraction of the total mass. The mean for M_{stars}/M_{dyn} is 0.11 and the mean for M_{gas}/M_{dyn} is 0.08. This is similar to the value found by Burlak (1996) of $M_{gas}/M_{stars} = 0.7$. Combining the gas and stellar mass numbers, we find that the mass in baryons for these dwarf galaxies is less than 20% the total mass, on average. Again, in agreement with a value of 26% from Burlak.

5. CONCLUSIONS

The paper is the third in a series concerning the properties of newly discovered LSB dwarfs. These galaxies were selected by irregular morphology from deep photographic plates (PSS-II). While the emphasis was on their visual appearance, this method to find new, uncataloged galaxies is automatically biased the search to objects with very low central surface brightnesses (i.e. not visible on previous sky surveys). The combination of low surface brightness and dwarf-like morphology was highly effective at producing a sample of low mass, low luminosity and small metric size galaxies. The results from the HI data presented herein can be summarized as the following:

- (1) Low mass dwarfs exists, but are rare. Contrary to claims (Briggs 1997), our current galaxy catalogs are incomplete for objects with HI masses less than $10^7 M_\odot$ since these objects are small and low in surface brightness and would be confused with Galactic emission in HI surveys.
- (2) The HI mass distribution has a mean of $M_{HI} = 7.9 \times 10^8 M_\odot$ with a sharp cutoff above $M_{HI} = 4.0 \times 10^9 M_\odot$ and a long tail to low HI masses. This distribution is much lower than a typical spiral sample and demonstrates that, although LSB galaxies are HI-rich, the gas component does not make them high mass. Mean HI surface densities are below the critical density for star formation based on the Toomre criteria, justifying statements that LSB dwarfs are inefficient at star formation and have quiescent past histories in agreement with their LSB nature.
- (3) LSB dwarfs continue the trend from late-type spirals of high M_{HI}/L , increasing with lower central surface brightnesses and bluer colors. The explanation of this correlation lies in a quiescent star formation history which leaves a large gas reservoir on top of a faint stellar population. Any recent star formation, even at a very low rate, has a sharp blueward effect on the underlying LSB structure.
- (4) The M_T^I, M_{dyn} correlation (Figure 7) demonstrates that the LSB dwarf sample that the dark matter (whether baryonic or non-baryonic) follows the baryonic matter. The distribution of M_{dyn}/L ranges from 1.5 to 50 (note that these are I band numbers, a factor of 4 higher than equivalent values in the B band).

The authors wish to thank the generous support of the Arecibo Observatory for the allocation of time to search for HI emission from the candidate dwarf galaxies and Michigan- Dartmouth-M.I.T Observatory in carrying out the photometry portion of this program This work is based on photographic plates obtained at the Palomar Observatory 48-inch Oschin Telescope for the Second Palomar Observatory Sky Survey which was funded by the Eastman Kodak Company, the National Geographic Society, the Samuel Oschin Foundation, the Alfred Sloan Foundation, the National Science Foundation and the National Aeronautics and Space Administration.

REFERENCES

- Ashman, K. 1992, *PASP*, 104, 1109
- Bicay, M. and Giovanelli, R. 1987, *AJ*, 93, 1326
- Binggeli, B., Tarengi, M. and Sandage, A. 1990, *A&A*, 228, 42
- Bothun, G., Beers, T., and Mould, J. 1985, *AJ*, 90, 2487
- Briggs, F. 1997, *ApJ*, 484, 618
- Burlak, M. 1996, *Astronomy Reports*, Vol. 40, p. 621
- Corbelli, E. and Salpeter, E. 1993, *ApJ*, 419, 104
- de Vaucouleurs, G. 1959, *Handb. der Physik*, 53, 275
- Eder, J., Oemler, A., Schombert, J. and Dekel, A. 1989, *ApJ*, 340, 29
- Giovanelli, R. and Haynes, M. 1988, in *Galactic and Extragalactic Radio Astronomy*, (New York:Springer-Verlag), p. 522
- Hoffman, L., Salpeter, E., Farhat, B., Roos, T., Williams, H. and Helou, G. 1996, *ApJS*, 105, 269
- Holmberg, E. 1957, *Medd. Lunds. Astron. Obs.*, Ser. II, No. 136
- Honma, M. 1999, *ApJ*, 516, 693
- Hunter, D. and Gallagher, J. 1986, *PASP*, 98, 5
- Impey, C., Sprayberry, D., Irwin, M. and Bothun, G. 1996, *ApJS*, 105, 209
- de Jong, R. 1996, *A&A*, 313, 45
- Kennicutt, R. 1989, *ApJ*, 344, 685
- Kennicutt, R. 1998, *ApJ*, 498, 541
- Lewis, B., Helou, G., and Salpeter, E. 1985, *ApJS*, 59, 161
- Lo, K., Sargent, W., and Young, K. 1993, *AJ*, 106, 507
- Matthews, L., van Driel, W. and Gallagher, J. 1998, *AJ*, 116, 1169
- McGaugh, S. 1992, *Ph.D. Thesis*, University of Michigan
- McGaugh, S., Schombert, J. and Bothun, G. 1995, *AJ*, 109, 2019
- McGaugh, S. and de Blok, W. 1997, *ApJ*, 481, 689
- Meurer, G., Carignan, C., Beaulieu, S. and Freeman, K. 1996, *AJ*, 111, 1551
- Salpeter, E. and Hoffman, G. 1996, *ApJ*, 465, 595
- Sandage, A. and Binggeli, B. 1984, *AJ*, 89, 919
- Schneider, S., Thuan, T., Magri, C. and Wadiak, J. 1990, *ApJS*, 72, 245
- Schneider, S. and Schombert, J. 1999, in press.
- Schombert, J. and Bothun, G. 1988, *AJ*, 95, 1389 (LSB1)
- Schombert, J., Bothun, G., Schneider, S., and McGaugh, S. 1992, *AJ*, 103, 1107 (LSB2)
- Schombert, J., Bothun, G., Impey, C. and Mundy, L. 1990, *AJ*, 100, 1523
- Schombert, J., Pildis, R., Eder, J. and Oemler, A. 1995, *AJ*, 110, 2067
- Schombert, J., Pildis, R. and Eder, J. 1997, *ApJS*, 111, 223

- Schombert, J., Eder, J. and McGaugh, S. 2000, in prep
- Shostak, G. 1975, ApJ, 198, 527
- Shostak, G. and van der Kruit, P. 1984, A&A, 132, 20
- Skillman, E., Terlevich, R. and van Woerden, H. 1988, A&A, 198, 33
- Skillman, E. and Kennicutt, R. 1993, ApJ, 411, 655
- Staveley-Smith, L., Davies, R. and Kinman, T. 1992, MNRAS, 258, 334
- Tammann, G. 1980, *Dwarf Galaxies*, ed. M. Tarenghi and K. Kjar (Geneva:ESO), 3
- Toomre, A. 1964, ApJ, 139, 1217
- Tully, R., Bottinelli, L., Gougenheim, L., Fisher, J., Sancisi, R. and van Woerden, H. 1978, A&A, 63, 37
- Turner, M. 1997, in *Dark matter in the Universe and its Direct Detection.*, ed. M. Minowa (Tokyo: Universal Academy Press), p. 83
- Worthey, G. 1994, ApJS, 95, 107
- de Vaucouleurs, G., de Vaucouleurs, A. and Corwin, H. 1976, *Second Reference Catalog of Bright Galaxies*, (Austin: University of Texas Press)
- van Zee, L., Haynes, M. and Giovanelli, R. 1995, AJ, 109, 990
- van Zee, L., Skillman, E. and Salzer, J. 1998, AJ, 116, 1186
- Zwaan, M., van der Hulst, J., de Blok, W. and McGaugh, S. 1995, MNRAS, 273, 35

Fig. 1.— HI profiles for the LSB dwarf sample. Baseline fits are shown as solid lines.

Fig. 2.— HI flux and profile widths (W_{50}) for the LSB dwarf sample. Most of the sample has widths below 150 km sec^{-1} . Galaxies with widths less than 40 km sec^{-1} would be indistinguishable from RFI.

Fig. 3.— Size and Velocity distributions for the LSB dwarf sample. The top panel displays the histogram scale lengths, α , from exponential fits to the dwarfs surface brightness profiles. For comparison, the mean scale length of a disk galaxy (de Jong 1996) is indicated. The bottom panel displays HI mass as a function of redshift. The solid line is the 3σ detection limit for a dwarf galaxy with a line width (W_{50}) of 75 km sec^{-1} . There appears to be no lower limit for HI mass for this sample.

Fig. 4.— The distribution of HI mass and HI surface density for the LSB dwarf sample. The sample has a mean value of $M_{HI} = 7.9 \times 10^8 M_{\odot}$ and a sharp cutoff at $M_{HI} = 4.0 \times 10^9 M_{\odot}$. The bottom panel displays mean HI surface density (Σ_{HI}) for each dwarf with available optical imaging. The critical threshold for star formation based on the Toomre (1964) instability criterion is between 9×10^{20} and $6 \times 10^{21} \text{ atoms cm}^{-2}$, which corresponds to the range of 5 and $30 M_{\odot} \text{ pc}^{-2}$ (van Zee *et al.* 1997).

Fig. 5.— The HI mass to light ratio for the LSB dwarf sample and the de Jong sample of spirals. In the top panel, M_{HI}/L is plotted against galaxy central surface brightness (μ_o). While the correlation is poor for the dwarfs, they do continue the spiral trend of increasing M_{HI}/L with decreasing surface brightness. The bottom panel plots M_{HI}/L versus galaxy color ($V - I$). Galaxies with highest M_{HI}/L values have the bluest $V - I$ colors, meaning that the portion of the stellar population that contributes a majority of the optical luminosity in a LSB dwarf galaxy is quite young.

Fig. 6.— The distribution of dynamical mass and total mass to light ratio for the LSB dwarf sample. The top panel displays the histogram of M_{dyn} values for dwarfs with optical imaging to determine scale length. The bottom panel displays the histogram for the dynamical (total) mass to light ratio based on I band magnitudes.

Fig. 7.— Dynamical mass versus total magnitude for the subset of the LSB dwarf sample with optical imaging. Lines of constant M/L are marked, as well as the boundary where the mass from stars equals the total mass (assuming $M_{stars}/L = 1.2$ (see text)).

Fig. 8.— Ratios of baryons from stars and gas to total mass for the LSB dwarf sample. The top two panels display the histograms of the ratio of mass from gas and stars (assuming standard corrections for helium, metals and M_*/L , see text). The bottom panel displays the histogram for the sum of the baryons from gas and stars divided by total mass. For a majority of LSB dwarfs, the mass in visible baryons is less than 20% the total mass of the galaxy.

Table 1. LSB Dwarf Galaxy Sample

Field	RA 1950	DEC 1950	V_h km s^{-1}	V_0 km s^{-1}	W km s^{-1}	D/S	F.I. mJy km s^{-1}	$\log M_{HI}$ M_\odot	run
(1)	(2)	(3)	(4)	(5)	(6)	(7)	(8)	(9)	(10)
409-1	000022.2	291821	4836	5074	114	D	1400	9.21	1
409-3	000204.9	291914	3
409-4	000328.4	270417	3181	3412	69	D:	1500	8.90	1
409-5	000452.7	314739	4864	5105	100	D	2100	8.90	1
409-6	000729.4	275704	3
409-7	001141.3	283710	7060	7291	167	:	1800	9.63	1
409-9	001256.3	282244	6682	6911	87	D	930	9.30	1
409-11	001349.5	271754	4597	4823	92	D	870	8.96	1
409-13	234841.0	324243	4951	5202	128	D	940	9.06	1
409-14	235711.5	265838	4699	4934	64	S	890	8.99	1
409-15	000639.0	301218	3
409-16	235004.7	305748	5161	5410	68	S	900	9.07	3
409-17	235557.0	302336	4811	5060	68	S	523	8.78	3
409-18	001348.5	301200	6904	7135	155	D	1835	9.62	3
409-19	001033.5	293730	7039	7270	138	:	638	9.18	3
409-20	001053.3	293648	3
474-1	003221.5	243454	5480	5689	121	D	610	8.95	1
474-4	004118.1	255225	4898	5105	38	S	950	9.05	1
474-5	004322.9	273108	3
474-7	004731.3	265708	4922	5123	119	D	905	9.03	3
474-9	005254.7	235529	4980	5174	82	D	1300	9.19	1
475-3	010146.0	221330	5662	5845	118	D	1200	9.27	1
475-4	011201.2	265223	3618	3807	111	D	4900	9.50	1
476-2	012118.1	264715	4908	5091	163	D	2800	9.51	1
476-3	012322.4	274231	4021	4205	75	D:	1100	8.94	1
476-4	012722.2	253628	3678	3856	152	D	9300	9.79	1
476-5	012837.2	234149	3414	3582	65	S	4400	9.40	1
476-6	013428.5	261057	3872	4044	66	D:	990	8.86	1
476-8	013929.3	260657	359	527	38	S	1100	7.14	1
476-9	014009.0	271848	3
495-1	081921.5	224606	2309	2215	75	D	389	7.93	2
495-2	082657.7	253930	2197	2116	34	S	669	8.13	2
495-3	082518.0	255724	2267	2188	50	S	546	8.07	2

Table 1—Continued

Field	RA 1950	DEC 1950	V_h km s ⁻¹	V_0 km s ⁻¹	W km s ⁻¹	D/S	F.I. mJy km s ⁻¹	log M_{HI} M_\odot	run
(1)	(2)	(3)	(4)	(5)	(6)	(7)	(8)	(9)	(10)
500-1	102116.1	263812	2
500-3	100311.3	240642	1347	1260	92	D	1048	7.87	2
500-4	101633.5	225712	1576	1486	67	S	395	7.59	2
500-5	101551.0	215724	4078	3983	178	D	2802	9.30	2
500-6	102513.7	222624	9346	9256	70	S	695	9.43	2
508-1	130325.8	275842	2527	2539	228	D	6128	9.25	2
508-2	130208.4	270248	1924	1931	84	S	3104	8.72	2
508-3	130032.4	262054	2
508-4	132152.8	253742	2
508-5	131049.8	243706	4406	4408	85	S	835	8.86	2
512-1	143436.0	275124	7199	7276	156	D	1082	9.41	2
512-2	143108.4	271300	831	903	75	S	2391	7.94	2
512-3	142851.0	264018	4201	4269	119	D:	761	8.80	2
512-4	143003.0	263236	4805	4874	102	D	2544	9.43	2
512-5	142954.6	260424	2
512-6	144321.6	255348	4269	4345	119	D	3717	9.50	2
512-7	144423.4	255448	4261	4338	127	D	2452	9.32	2
512-8	142605.4	251612	2
512-9	143744.4	243424	4499	4566	119	D	1819	9.23	2
512-10	143630.6	232906	4526	4588	76	S	528	8.70	2
512-11	144631.2	231200	2
512-12	144404.8	225312	2
514-1	151929.4	275706	2
514-2	152820.4	272612	2023	2139	33	S	1591	8.52	2
514-3	151745.6	262842	2
514-4	151753.4	262848	2
514-5	152146.2	242336	6579	6680	69	D	573	9.06	2
514-6	152618.6	243406	2
516-1	161228.8	272206	2
516-2	160836.0	255012	9767	9910	132	D	610	9.43	2
516-3	160557.0	242612	9750	9886	35	S	672	9.47	2
516-4	160930.6	241542	9322	9460	44	S	370	9.17	2
535-1	225457.9	274242	2944	3207	108	D	2400	9.05	1

Table 1—Continued

Field	RA 1950	DEC 1950	V_h km s ⁻¹	V_0 km s ⁻¹	W km s ⁻¹	D/S	F.I. mJy km s ⁻¹	log M_{HI} M_\odot	run
(1)	(2)	(3)	(4)	(5)	(6)	(7)	(8)	(9)	(10)
535-2	225636.1	260907	7705	7964	65	D	840	9.38	1
535-3	225702.6	245132	7417	7673	75	D:	730	9.29	1
535-4	230114.7	232459	1155	1406	94	D	2700	8.38	1
535-5	230354.6	273713	6913	7173	68	S	530	9.09	1
535-6	230552.2	272647	2884	3143	86	D	2900	9.11	1
535-8	231651.8	243937	5809	6057	94	D	1500	9.39	1
535-9	231913.4	272316	5935	6188	45	S:	940	9.21	1
538-1	000014.4	184122	713	924	50	S	1100	7.63	1
538-2	000156.8	202620	2175	2383	84	S:	1977	8.70	3
538-3	000213.0	180156	6315	6523	77	D:	1000	9.28	1
538-4	000325.9	213506	3
538-7	000839.5	225554	3
538-11	001021.1	181543	5514	5718	32	S	490	8.86	1
538-12	001118.3	230333	3
538-15	235256.9	173829	1769	1981	150	D	15000	9.42	1
538-16	235312.9	180853	1739	1953	94	D	6200	9.03	1
538-17	235706.6	172137	6457	6666	174	D	1200	9.38	1
538-18	235903.9	171238	6413	6621	72	S:	850	9.22	1
539-1	001428.9	224311	4405	4619	118	D	2200	9.32	1
539-2	001440.6	171450	1005	1204	72	D	2200	8.16	1
539-3	001444.1	203136	4366	4574	144	D	5000	9.67	1
539-4	001613.7	194245	5542	5747	72	S	1400	9.32	1
539-5	001805.3	221855	7352	7563	197	D	3500	9.95	1
539-6	001822.7	172447	5235	5432	136	D	1500	9.30	1
539-8	002152.2	204642	5246	5451	76	D	580	8.89	1
540-1	002958.9	221817	4560	4764	118	D	1100	9.05	1
540-2	003804.7	222406	5899	6098	73	D	660	9.04	1
540-3	004333.6	191221	2646	2832	231	D	18000	9.81	1
540-4	004417.8	211818	5180	5372	72	S	1200	9.19	1
540-8	005404.3	225008	2594	2778	92	D	1169	8.61	3
541-4	010559.6	211529	5546	5723	100	D	1700	9.40	1
559-1	071941.3	172112	2
559-2	072650.3	191330	2

Table 1—Continued

Field	RA 1950	DEC 1950	V_h km s ⁻¹	V_0 km s ⁻¹	W km s ⁻¹	D/S	F.I. mJy km s ⁻¹	log M_{HI} M_\odot	run
(1)	(2)	(3)	(4)	(5)	(6)	(7)	(8)	(9)	(10)
559-3	073215.0	191830	8580	8482	576	D	4144	10.13	2
559-4	071904.7	205054	2
559-5	071515.5	211054	2
559-6	072218.5	221048	2
561-1	075748.0	200006	7714	7612	95	D	1585	9.62	2
561-2	080345.0	190736	4631	4523	85	D	866	8.90	2
563-1	085319.1	172706	4161	4037	34	S	531	8.59	2
563-2	085012.5	183742	4319	4201	119	D	3928	9.49	2
563-3	084348.0	190430	3935	3820	85	D:	940	8.79	2
563-4	085215.0	195630	3495	3384	110	D	5097	9.42	2
563-5	083357.5	195042	4645	4535	110	D	2700	9.40	2
563-6	084936.5	211230	3567	3462	110	D	321	8.24	2
564-1	085455.1	224942	2
564-2	091146.1	230000	8131	8034	70	D	231	8.83	2
564-4	090603.5	213400	2703	2599	109	D	557	8.23	2
564-5	085417.3	210048	2
564-6	085628.7	204536	2
564-7	090227.5	204148	2
564-8	090001.7	201630	488	378	58	S	1819	7.07	2
564-10	090628.1	183536	2
564-11	090423.3	180300	4284	4163	153	D	952	8.87	2
564-12	085723.3	174648	3840	3718	144	D	2266	9.15	2
564-13	090027.5	173318	4292	4169	153	D:	433	8.53	2
564-14	090547.3	174218	2
564-15	090830.5	172242	3386	3262	135	D	1125	8.73	2
564-16	090825.1	201054	6873	6762	35	D	237	8.69	2
564-17	085408.3	203106	2
565-1	091509.0	224912	6239	6141	103	D	1092	9.27	2
565-2	092139.0	222918	3830	3731	110	D	6472	9.61	2
565-3	093448.5	221524	7623	7523	165	D	999	9.41	2
565-4	093326.3	215212	2
565-5	092958.7	214118	558	455	364	D	4659	7.64	2
565-7	093657.5	210906	2
565-8	093822.7	205500	2

Table 1—Continued

Field	RA 1950	DEC 1950	V_h km s ⁻¹	V_0 km s ⁻¹	W km s ⁻¹	D/S	F.I. mJy km s ⁻¹	log M_{HI} M_\odot	run
(1)	(2)	(3)	(4)	(5)	(6)	(7)	(8)	(9)	(10)
565-9	093024.5	204430	2
565-10	092724.0	201300	561	451	33	S	732	6.83	2
565-11	093117.3	200518	2
565-12	091516.1	194236	2
565-13	091842.0	193636	2
565-14	091725.1	180648	2
565-15	093134.7	180448	2
565-16	093710.7	173412	2
568-2	104214.4	210730	1219	1128	33	S	594	7.53	2
568-3	102118.0	212030	5731	5635	128	D:	1604	9.36	2
568-4	101812.0	202424	1557	1455	75	D	1293	8.09	2
568-5	103006.0	193324	2
570-1	112234.1	170936	1021	927	50	S	783	7.48	2
570-2	112225.7	172148	2
570-3	112022.1	174448	1383	1290	67	D	465	7.54	2
570-4	111542.0	175812	1057	963	66	S	1860	7.89	2
570-5	111333.5	181336	2
570-6	112103.5	193254	1894	1810	92	D	189	7.44	2
570-7	111938.3	210900	810	733	50	S	1066	7.41	2
570-8	110057.5	224742	2
571-1	113436.0	212948	2
571-2	114551.6	203954	6796	6729	60	S	888	9.26	2
571-3	113548.6	201530	6981	6907	147	D:	1331	9.46	2
571-4	112022.2	194524	2
571-5	112104.8	193300	6132	6048	77	D:	230	8.58	2
571-6	112613.8	183324	2
571-7	113452.2	183542	2
571-8	113134.8	172542	2
572-1	114815.5	172518	2
572-2	115201.7	175642	3746	3670	144	D:	721	8.64	2
572-3	114855.7	173812	2
572-4	120458.1	185754	793	729	50	S	877	7.32	2
572-5	114539.2	185536	976	901	66	S	2198	7.90	2
572-6	115532.3	210700	4074	4014	59	S	1743	9.10	2

Table 1—Continued

Field	RA 1950	DEC 1950	V_h km s ⁻¹	V_0 km s ⁻¹	W km s ⁻¹	D/S	F.I. mJy km s ⁻¹	log M_{HI} M_\odot	run
(1)	(2)	(3)	(4)	(5)	(6)	(7)	(8)	(9)	(10)
572-7	115225.1	210012	2
575-1	124918.6	220042	580	557	33	S	2386	7.52	2
575-2	124953.4	215430	764	741	116	D:	8329	8.31	2
575-3	130016.2	221554	2
575-4	130010.1	221454	2
575-5	125313.2	192848	419	387	48	S	4373	7.47	2
575-6	124549.2	185442	2
575-7	125607.2	180454	1013	977	75	S	2463	8.02	2
575-8	130201.2	180742	2
575-9	130414.4	181600	2
576-1	132110.7	221006	7096	7095	216	D	1541	9.54	2
576-2	132549.8	210736	2
576-3	131146.1	204700	6504	6491	78	S	650	9.09	2
576-4	131419.7	203254	2
576-5	131407.7	203142	2
576-6	130733.5	195906	3731	3711	110	D	3941	9.39	2
576-7	131344.3	190136	6553	6534	69	D:	720	9.14	2
576-8	132219.7	192530	7165	7154	190	D	2202	9.70	2
576-9	131255.7	181554	3831	3808	110	D	1262	8.92	2
576-10	132914.3	171724	2
576-11	132424.0	201400	7168	7161	52	D	2559	9.77	2
577-1	134510.2	204142	2
577-2	133457.0	193106	6545	6543	95	D	1410	9.43	2
577-3	133040.2	183936	6936	6928	121	D	643	9.14	2
577-4	133355.8	182448	7080	7073	78	S	1388	9.49	2
577-5	133815.0	172054	4095	4087	110	D	1541	9.06	2
577-6	134625.2	173200	7572	7571	61	S	602	9.19	2
582-1	153153.4	215754	7065	7166	276	D	2330	9.73	2
582-2	152340.8	204824	4575	4665	51	D	273	8.43	2
582-3	153319.8	204824	2
582-4	153528.2	205700	4465	4565	85	D	302	8.45	2
582-5	151559.4	184918	2
584-1	160931.1	170030	4669	4783	85	D	1533	9.20	2

Table 1—Continued

Field	RA 1950	DEC 1950	V_h km s ⁻¹	V_0 km s ⁻¹	W km s ⁻¹	D/S	F.I. mJy km s ⁻¹	log M_{HI} M_\odot	run
(1)	(2)	(3)	(4)	(5)	(6)	(7)	(8)	(9)	(10)
584-2	155935.3	185200	2628	2741	109	D	2051	8.84	2
584-3	161520.3	193854	2576	2704	126	D	1746	8.76	2
584-4	155515.5	204842	2269	2385	167	D	7885	9.30	2
584-5	161913.1	205900	3104	3239	135	D	8027	9.58	2
584-6	160613.7	211918	4787	4913	85	S	2147	9.37	2
584-7	155816.7	211824	2
609-2	003545.3	131220	5597	5770	102	:	660	8.99	1
609-3	003548.3	131244	5459	5632	158	:	1600	9.36	1
609-4	004217.2	163957	4678	4845	196	D	2234	9.37	3
609-5	005210.2	132325	5428	5590	66	S	1300	9.26	1
611-5	011706.5	163148	2163	2318	32	S	1200	8.46	1
611-6	011823.7	164844	2495	2650	142	D	4381	9.14	3
611-7	011838.9	120902	644	783	103	D:	12000	8.52	1
611-10	012038.9	170143	5806	5961	214	D	1326	9.33	3
611-11	012235.0	135352	5041	5183	35	S	1200	9.16	1
611-13	012432.9	132036	4505	4643	102	D	2500	9.38	1
611-14	012606.4	162555	594	742	49	S	2200	7.74	1
611-15	012725.5	132031	6395	6531	120	D	1800	9.54	1
611-16	012734.8	142511	2449	2589	121	D	3800	9.06	1
611-17	012855.9	130429	2739	2873	107	D	820	8.48	1
611-18	012905.9	135354	6763	6900	175	D	2300	9.69	1
611-21	013125.1	123501	5019	5149	104	D	860	9.01	1
631-1	075950.3	160900	4698	4577	136	D	1593	9.18	2
631-2	080813.1	151400	2
631-3	080246.7	145448	2
631-4	075945.5	144812	2
631-5	075731.1	145054	2
631-6	075405.4	144630	2
631-7	075413.7	143118	343	216	83	S	15390	7.51	2
631-8	075707.7	135848	4471	4340	127	D	929	8.90	2
631-9	075439.0	124018	2
631-10	075653.3	121248	2
631-11	080854.0	120536	2
634-1	085429.3	131448	2

Table 1—Continued

Field	RA 1950	DEC 1950	V_h km s ⁻¹	V_0 km s ⁻¹	W km s ⁻¹	D/S	F.I. mJy km s ⁻¹	log M_{HI} M_\odot	run
(1)	(2)	(3)	(4)	(5)	(6)	(7)	(8)	(9)	(10)
634-2	090130.0	134024	2
634-3	090607.7	144706	318	181	33	S	217	5.50	2
634-5	090039.0	155048	2
634-6	085718.0	162348	2
634-7	085018.5	164848	2
637-1	095013.1	172348	2
637-2	095431.1	175948	2
637-3	095857.5	175554	2227	2110	92	D	1538	8.49	2
637-4	095054.5	163400	2
637-5	095458.7	160742	7727	7600	148	D	977	9.40	2
637-6	095806.0	154506	2
637-7	095328.7	155054	4580	4452	136	D	2330	9.32	2
637-8	100049.7	161600	7818	7693	87	D	1063	9.45	2
637-9	095913.8	160012	2
637-10	100914.3	163106	2
637-11	100954.0	154648	2
637-12	100642.0	151800	2
637-13	095858.2	151124	2
637-14	100031.1	145224	2
637-15	100701.7	142018	10772	10639	142	D	1313	9.83	2
637-16	100949.1	135948	11401	11267	71	D:	967	9.74	2
637-17	085524.5	140118	7492	7352	113	D	1850	9.65	2
637-18	100454.0	132106	2740	2602	42	S	1469	8.65	2
637-19	095250.3	130136	2
637-20	095927.5	123636	6497	6355	86	D	2067	9.57	2
637-22	095209.0	120036	2
640-2	105049.2	170306	1093	985	91	S	18530	8.91	2
640-3	105049.2	170306	2
640-4	105049.2	170306	2
640-5	110937.8	160148	2
640-6	104737.2	161424	2
640-7	104758.8	160148	1115	1001	100	D	3764	8.23	2
640-8	105813.8	140918	2
640-9	110333.6	130636	2
640-10	104742.0	133200	2
640-11	104822.8	133542	6783	6658	155	D:	231	8.66	2

Table 1—Continued

Field	RA 1950	DEC 1950	V_h km s ⁻¹	V_0 km s ⁻¹	W km s ⁻¹	D/S	F.I. mJy km s ⁻¹	log M_{HI} M_\odot	run
(1)	(2)	(3)	(4)	(5)	(6)	(7)	(8)	(9)	(10)
640-12	105317.4	123624	2
640-13	105337.2	121642	990	861	42	S	1218	7.61	2
640-14	105533.6	121548	2
640-15	110808.4	121718	3244	3121	211	D	4534	9.30	2
640-16	105225.2	142154	2
646-1	130206.0	180148	2
646-2	130727.6	172536	3580	3549	135	D	3311	9.27	2
646-3	125301.8	160018	2
646-4	125355.8	152130	2
646-5	125030.0	144024	1044	990	91	D	2496	8.04	2
646-6	125026.4	143942	2
646-7	125609.6	142912	213	162	33	S	6968	6.92	2
646-8	124933.0	131042	2101	2040	50	S:	117	7.34	2
646-9	125042.0	125424	1817	1755	50	S	1452	8.30	2
646-10	125924.0	131136	2
646-11	125412.0	121230	565	503	58	S	2025	7.36	2
648-1	134239.5	124048	2
648-2	134451.0	133300	2
648-3	135222.1	171954	6990	6993	181	D	1601	9.55	2
648-4	134624.0	173200	7575	7574	69	S	482	9.09	2
648-6	133427.5	173024	2
651-1	142737.2	175436	2
651-2	142909.6	172524	2
651-3	144612.6	163842	2
651-4	145123.4	160212	6299	6345	129	D	1162	9.32	2
651-5	144740.8	152936	2
651-6	144306.0	135648	2
651-7	144203.0	124248	2
651-8	144404.2	121924	2
656-1	162554.0	174500	4530	4660	60	S	1333	9.11	2
656-2	161104.2	171918	1090	1207	100	D	4107	8.43	2
656-4	161405.4	161242	2
656-5	161527.6	154906	8950	9065	201	D	970	9.55	2
656-6	161419.2	142942	2

Table 1—Continued

Field	RA 1950	DEC 1950	V_h km s ⁻¹	V_0 km s ⁻¹	W km s ⁻¹	D/S	F.I. mJy km s ⁻¹	log M_{HI} M_\odot	run
(1)	(2)	(3)	(4)	(5)	(6)	(7)	(8)	(9)	(10)
681-1	002859.6	085342	2156	2319	108	D	5900	9.15	1
681-4	004002.0	094350	5071	5229	63	D:	460	8.75	1
681-5	004035.6	083256	5363	5517	110	D:	660	8.96	1
681-8	004822.4	072543	5274	5428	128	D	492	8.81	3
685-1	014801.1	115434	6873	6988	166	D	1900	9.62	1
685-4	014906.0	113919	4839	4952	188	D	4600	9.71	1
685-6	015049.2	123451	4656	4771	84	D	630	8.81	1
685-7	015206.7	101908	6085	6191	37	S	2200	9.58	1
685-8	015220.7	103641	6205	6312	193	D	1600	9.46	1
685-11	015427.1	111712	3470	3578	112	D:	2800	9.21	1
685-14	015702.8	101032	6302	6403	77	D:	1100	9.31	1
685-15	015703.4	120251	7828	7936	145	D	1500	9.63	1
685-16	015822.0	081524	7804	7897	147	D	1900	9.73	1
685-18	015919.6	112922	4643	4747	136	D	1200	9.09	1
685-19	020009.4	073432	5727	5816	94	D	806	9.09	1
685-20	020550.3	120608	3
685-21	020940.8	125817	2224	2325	50	S:	917	8.35	1
685-22	021222.4	083553	1590	1673	38	S	1000	8.10	1
702-1	072816.7	080624	1879	1732	84	D:	2774	8.57	2
702-2	073210.7	110154	2
704-1	082334.1	111200	2
704-2	082048.5	101236	4236	4083	170	D	2756	9.32	2
704-3	081924.5	082730	4174	4014	76	S:	1169	8.93	2
704-4	081633.5	120236	2
709-2	100139.5	123730	2
709-3	095902.3	114742	7169	7023	138	D	538	9.08	2
709-4	095827.0	111612	2
709-5	095007.7	112336	9472	9323	88	D:	530	9.32	2
709-6	095551.5	102518	5228	5075	77	D	300	8.54	2
709-7	100454.5	101300	7561	7398	69	S	678	9.22	2
709-8	095846.7	091724	2
709-9	095018.5	081548	2642	2479	126	D	3350	8.97	2
709-10	095023.3	080106	2594	2430	34	S	420	8.05	2

Table 1—Continued

Field	RA 1950	DEC 1950	V_h km s ⁻¹	V_0 km s ⁻¹	W km s ⁻¹	D/S	F.I. mJy km s ⁻¹	log M_{HI} M_\odot	run
(1)	(2)	(3)	(4)	(5)	(6)	(7)	(8)	(9)	(10)
709-11	095657.0	120048	2993	2848	59	S:	221	7.91	2
709-12	095207.1	120012	2
721-1a	135754.6	123748	5722	5710	111	D	888	9.11	2
721-1	135754.6	123748	6109	6097	69	D	1582	9.42	2
721-2	135940.2	112148	2
721-3	141106.6	110718	2
721-4	140028.8	105148	2
721-5	140017.4	101400	5815	5795	94	D	964	9.16	2
721-7	140359.4	093600	7205	7186	69	S:	1637	9.58	2
721-8	135836.6	092054	5433	5408	103	D:	1036	9.13	2
721-9	135833.0	090100	2
721-10	135328.8	091436	2
721-11	135404.2	084000	2
721-12	135107.2	083554	6942	6908	112	D	861	9.27	2
721-14	140213.2	090136	1196	1173	91	D	5716	8.55	2
721-15	141042.0	085100	7393	7376	138	D	5590	10.14	2
721-16	140038.4	082842	5260	5234	94	D:	1018	9.10	2
721-17	135516.8	080454	2
723-1	143121.6	130418	2
723-2	144204.2	124236	2
723-3	142857.0	122706	7919	7932	78	D:	1343	9.58	2
723-4	143004.8	114618	2166	2177	109	D	3487	8.87	2
723-5	143415.6	114736	1788	1803	100	D:	1051	8.19	2
723-6	143255.8	084330	2092	2094	125	D	2473	8.69	2
723-7	145003.6	102400	6922	6945	164	D	2622	9.75	2
723-8	144806.6	083430	2
723-9	144254.6	080254	1690	1774	33	S	4311	8.79	2
749-2	230835.7	110540	2639	2853	69	S	1500	8.74	1
749-3	231011.8	102729	6579	6790	129	D	1700	9.55	1
749-4	231017.4	121322	4891	5108	142	D	1800	9.32	1
749-6	231455.1	072139	3872	4071	91	D	3500	9.42	1
749-7	231504.3	092254	3811	4016	127	D	1400	9.01	1
749-8	231517.4	110905	3794	4005	68	S:	366	8.42	3
749-9	231625.2	073021	4310	4508	102	D:	820	8.87	1
749-10	231638.7	072550	3762	3960	159	D	3600	9.40	1

Table 1—Continued

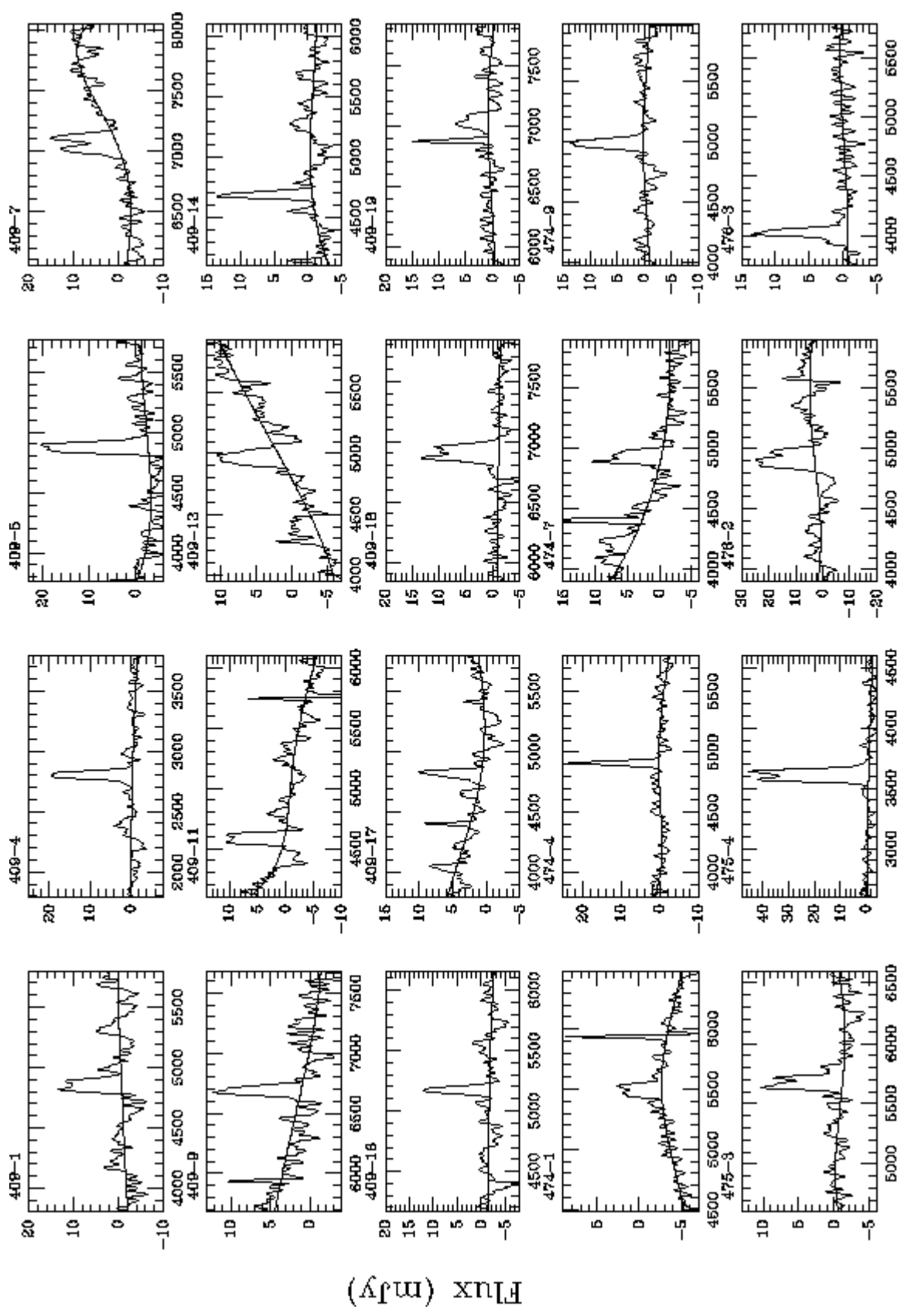
Field	RA 1950	DEC 1950	V_h km s^{-1}	V_0 km s^{-1}	W km s^{-1}	D/S	F.I. mJy km s^{-1}	$\log M_{HI}$ M_\odot	run
(1)	(2)	(3)	(4)	(5)	(6)	(7)	(8)	(9)	(10)
749-11	231639.2	094449	3
749-12	231941.4	090632	3574	3776	83	D	2700	9.24	1
749-13	232005.4	100635	3521	3727	127	D	1700	9.03	1
749-14	232015.5	112954	3836	4046	154	D	2000	9.17	1
749-15	232639.9	113428	3648	3855	76	D:	1800	9.08	1
749-17	233211.3	123909	3838	4046	119	D	1200	8.95	1
774-1	074700.0	064418	4953	4793	162	D	2720	9.45	2
774-2	074540.7	041342	5555	5385	137	D	1740	9.36	2
774-3	073928.1	030524	7417	7245	156	D	2370	9.75	2
822-4	233641.6	040800	6391	6567	197	D	1857	9.56	1
822-6	233736.1	070153	3699	3885	92	D:	2600	9.25	1
822-7	233840.1	053849	1732	1913	86	D:	1700	8.45	1
822-9	234108.9	062402	3809	3991	138	D	1000	8.86	1
822-10	234250.4	063315	5308	5490	84	D	1700	9.36	1
822-11	234259.8	060813	4421	4597	178	D:	1554	9.17	3
822-14	234646.8	035412	2971	3141	73	D:	570	8.40	1
822-17	234811.6	034227	2907	3077	42	S	1362	8.76	3

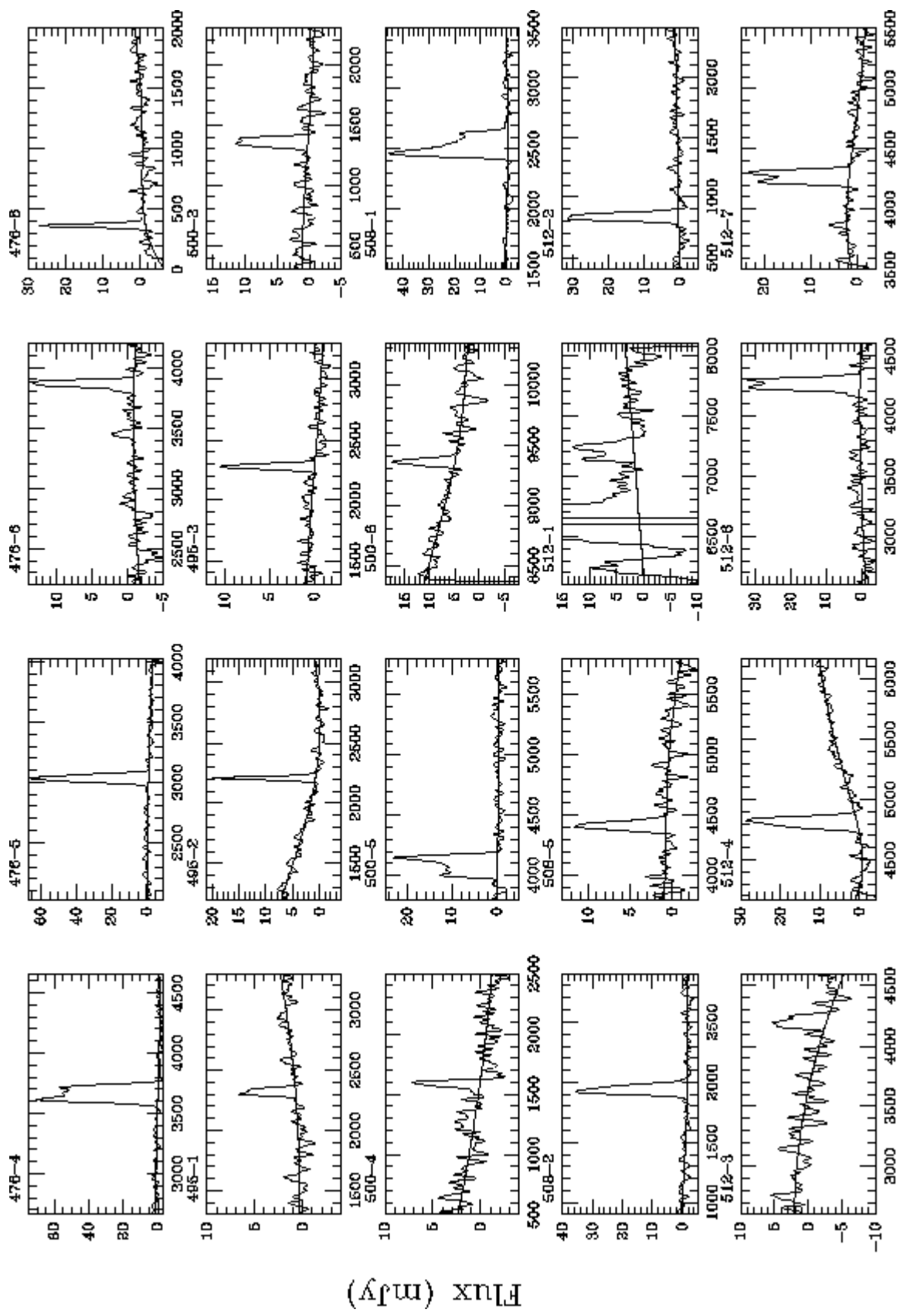
Table 2. Optical and Mass Parameters

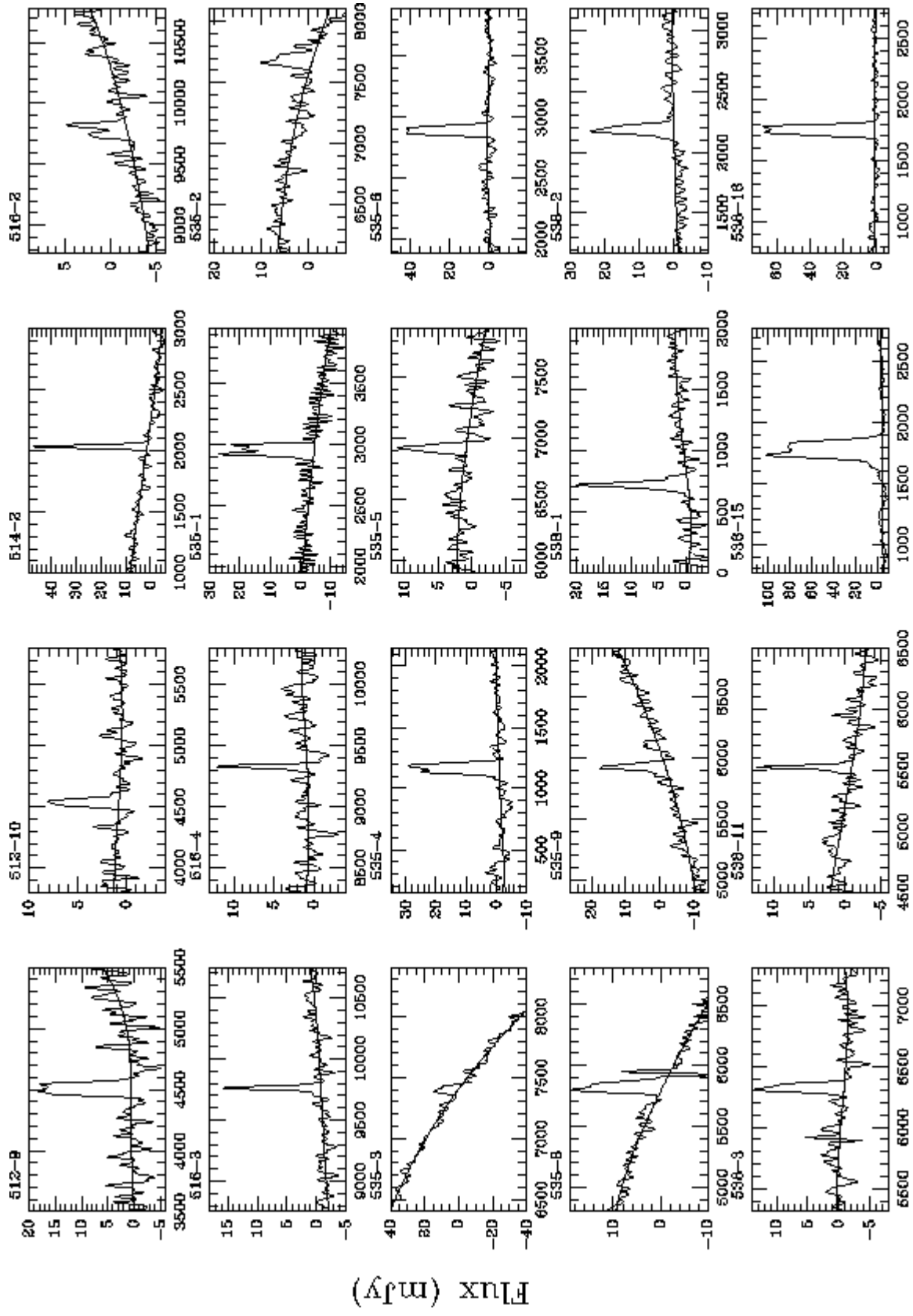
Name	Radius (arcsec)	b/a	M_I	$\log \Sigma_{HI}$ ($M_\odot \text{ pc}^{-2}$)	$\log M_{dyn}$ (M_\odot)
(1)	(2)	(3)	(4)	(5)	(6)
476-8	16.0	0.53	-13.9	4.84	8.05
495-1	15.6	0.59	-16.4	1.60	9.21
495-2	14.2	0.76	-16.3	2.60	8.60
495-3	22.1	0.54	-15.6	1.23	8.98
500-3	17.3	0.60	-16.3	3.44	9.22
500-4	14.1	0.66	-16.4	1.78	8.93
500-5	22.8	0.51	-19.0	6.27	10.44
508-2	25.8	0.76	-17.4	3.68	9.65
508-5	16.8	0.74	-18.0	2.36	9.80
512-2	25.4	0.50	-15.9	4.38	8.99
512-3	12.0	0.48	-17.0	6.62	9.78
512-7	12.8	0.82	-17.7	10.93	10.23
512-9	17.7	0.73	-18.5	4.71	10.18
512-10	11.6	0.61	-17.0	3.84	9.43
563-1	14.7	0.83	-17.4	1.76	8.92
563-4	26.2	0.57	-18.1	7.76	9.99
563-5	18.1	0.37	-18.3	13.32	9.86
564-4	14.6	0.62	-16.8	2.52	9.65
564-8	15.1	0.83	-13.4	5.75	8.41
564-11	7.3	0.57	-15.7	18.62	9.85
564-12	16.9	0.57	-18.1	8.30	10.11
564-15	18.1	0.53	-17.6	3.84	9.99
565-1	11.5	0.36	-18.3	13.71	9.73
565-10	22.0	0.85	-13.8	1.07	8.13
568-2	13.1	0.64	-19.0	3.21	8.25
568-4	24.4	0.85	-17.1	1.52	9.54
570-4	24.8	0.68	-15.5	2.65	8.99
572-2	9.9	0.23	-16.2	19.01	9.73
572-4	13.5	0.80	-15.0	3.57	8.44
572-5	17.4	0.66	-15.3	6.47	8.79
575-1	26.6	0.51	-13.6	3.91	8.25
575-2	40.1	0.49	-16.6	6.24	9.52
575-5	24.6	0.44	-12.0	9.79	8.22
575-7	17.3	0.57	-15.2	8.50	8.89
576-9	13.4	0.64	-16.6	6.60	9.80
577-2	12.6	0.64	-18.2	8.18	9.86
577-5	15.7	0.61	-17.6	6.04	9.88
582-1	8.4	0.36	-16.9	54.44	10.61

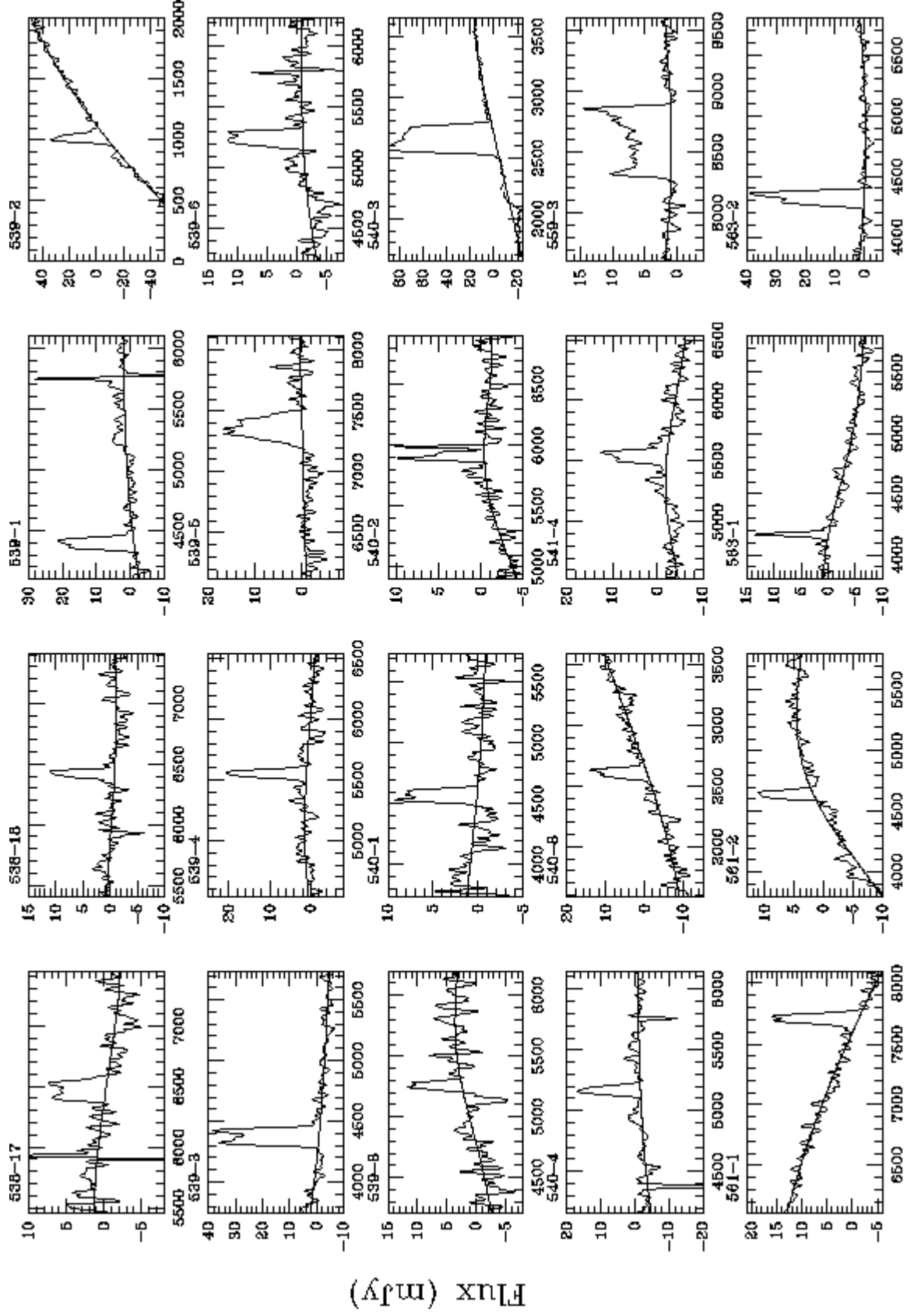
Table 2—Continued

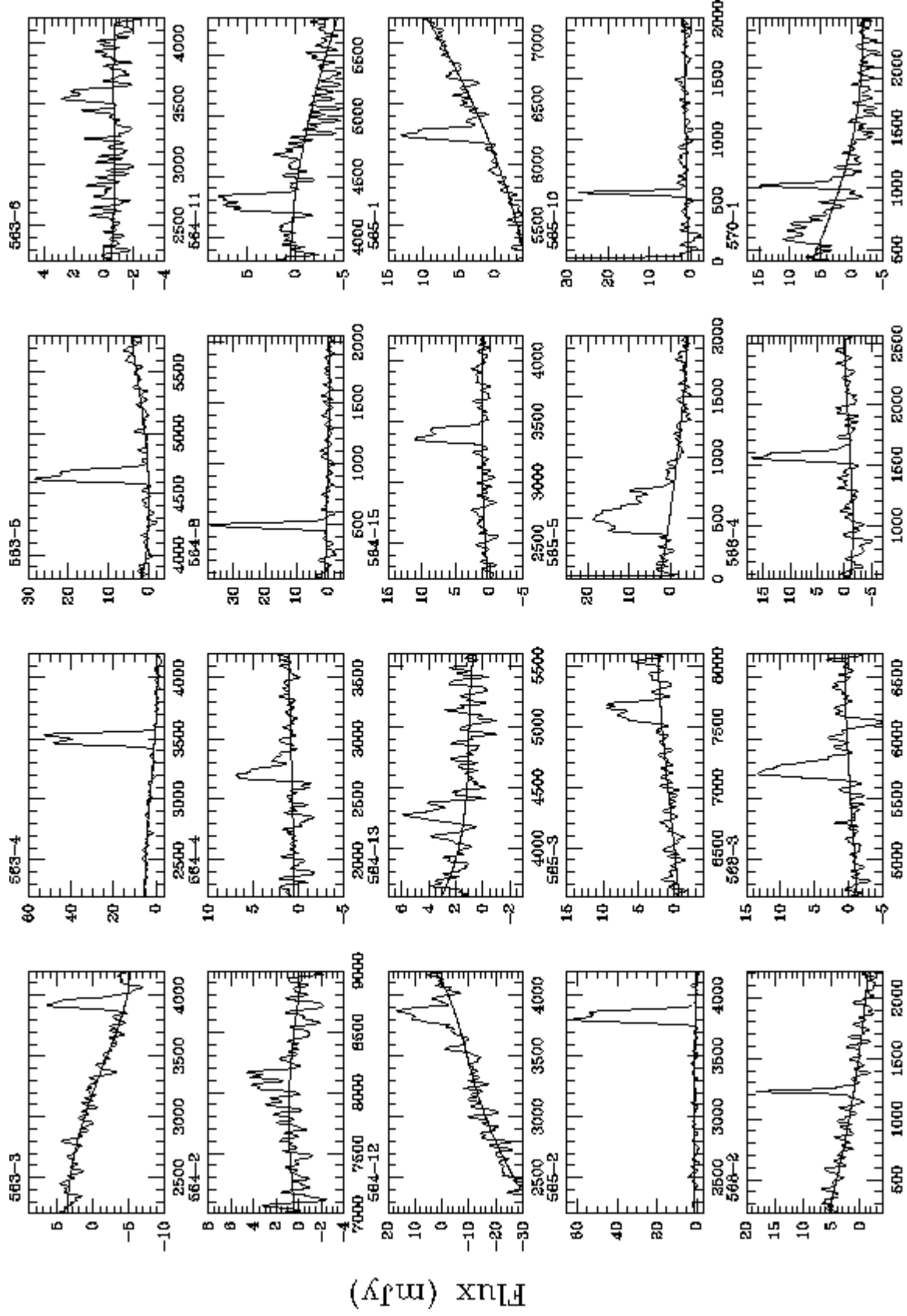
Name	Radius (arcsec)	b/a	M_I	$\log \Sigma_{HI}$ ($M_{\odot} \text{ pc}^{-2}$)	$\log M_{dyn}$ (M_{\odot})
(1)	(2)	(3)	(4)	(5)	(6)
582-2	8.1	0.87	−16.5	2.87	9.16
584-2	21.3	0.62	−17.5	4.33	9.84
584-3	17.3	0.49	−16.6	7.10	9.80
584-4	23.8	0.38	−17.5	21.55	10.11
631-1	18.5	0.69	−18.5	4.05	10.29
631-7	42.5	0.44	−14.4	11.54	8.66
631-8	11.5	0.64	−17.0	6.59	9.94
637-18	21.0	0.82	−16.9	2.41	9.04
640-7	15.5	0.47	−15.5	19.85	9.09
640-13	21.1	0.68	−14.5	2.40	8.48
646-2	13.8	0.67	−17.5	15.32	10.02
646-7	65.3	0.59	−12.2	1.67	8.11
646-8	9.2	0.48	−15.0	1.71	8.55
646-11	25.3	0.85	−13.0	2.20	8.80
656-2	31.0	0.52	−16.0	4.89	9.49
702-1	18.5	0.89	−16.3	5.38	9.73
704-3	15.4	0.58	−17.3	5.08	9.47
709-10	14.1	0.68	−16.0	1.86	8.64
709-11	9.3	0.47	−15.2	3.26	8.83
721-5	13.8	0.69	−17.7	4.33	9.89
721-16	15.3	0.71	−18.2	3.66	9.91
723-5	27.0	0.58	−17.5	1.49	9.64
723-6	17.4	0.36	−16.3	13.55	9.63
723-9	36.1	0.44	−17.6	4.52	8.88
774-2	15.6	0.39	−18.3	11.01	10.09
774-3	17.2	0.75	−18.6	6.38	10.67

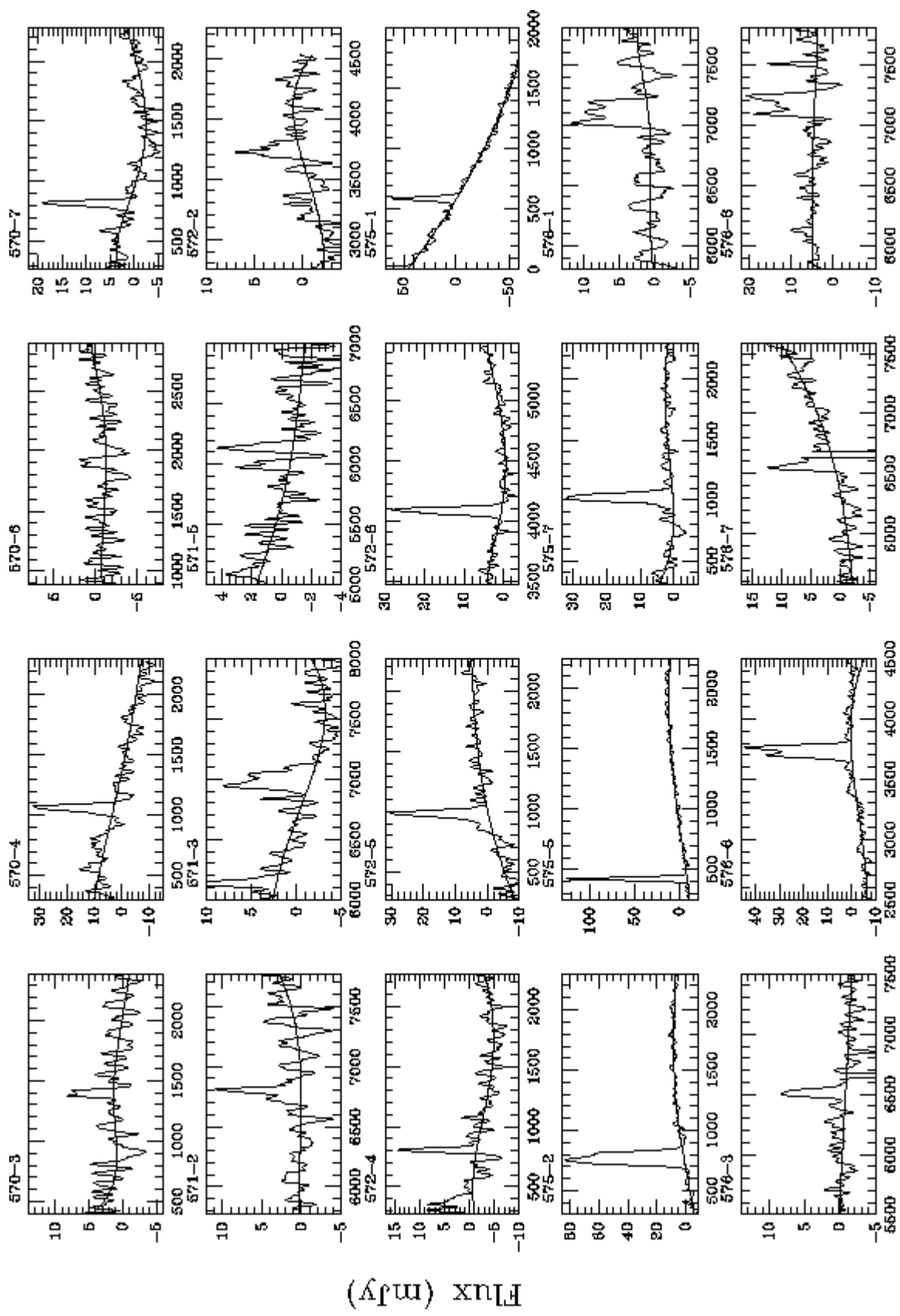


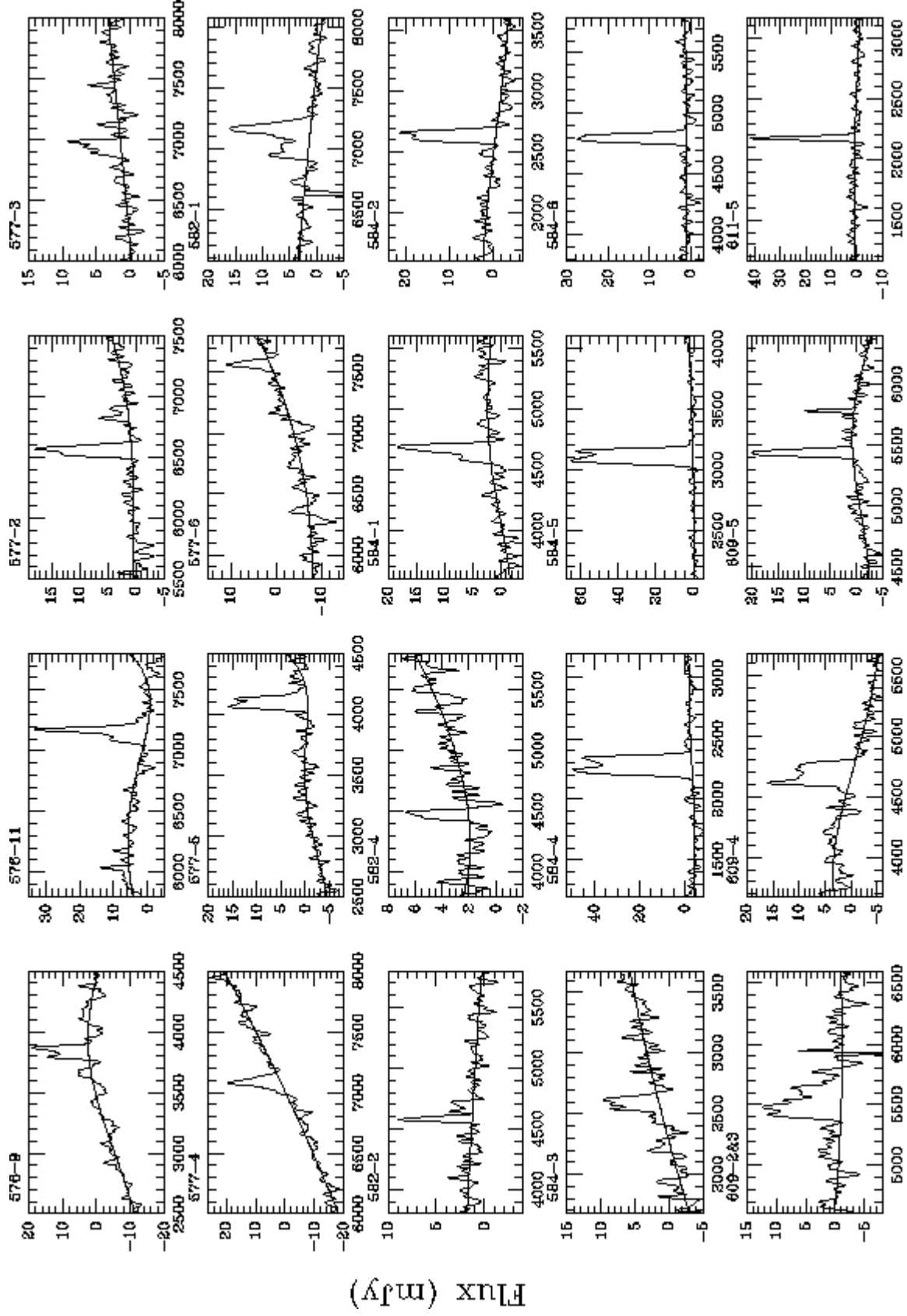




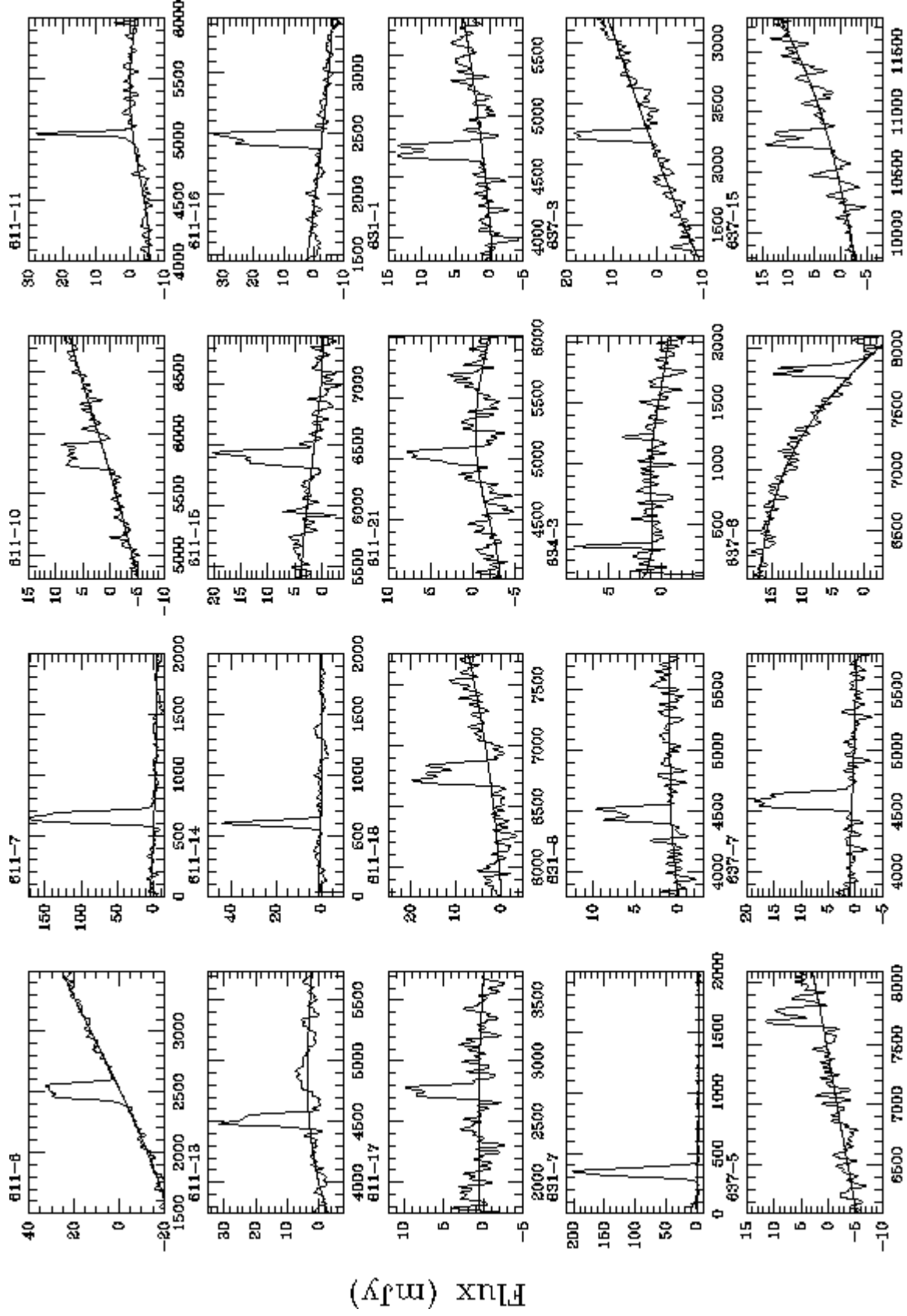




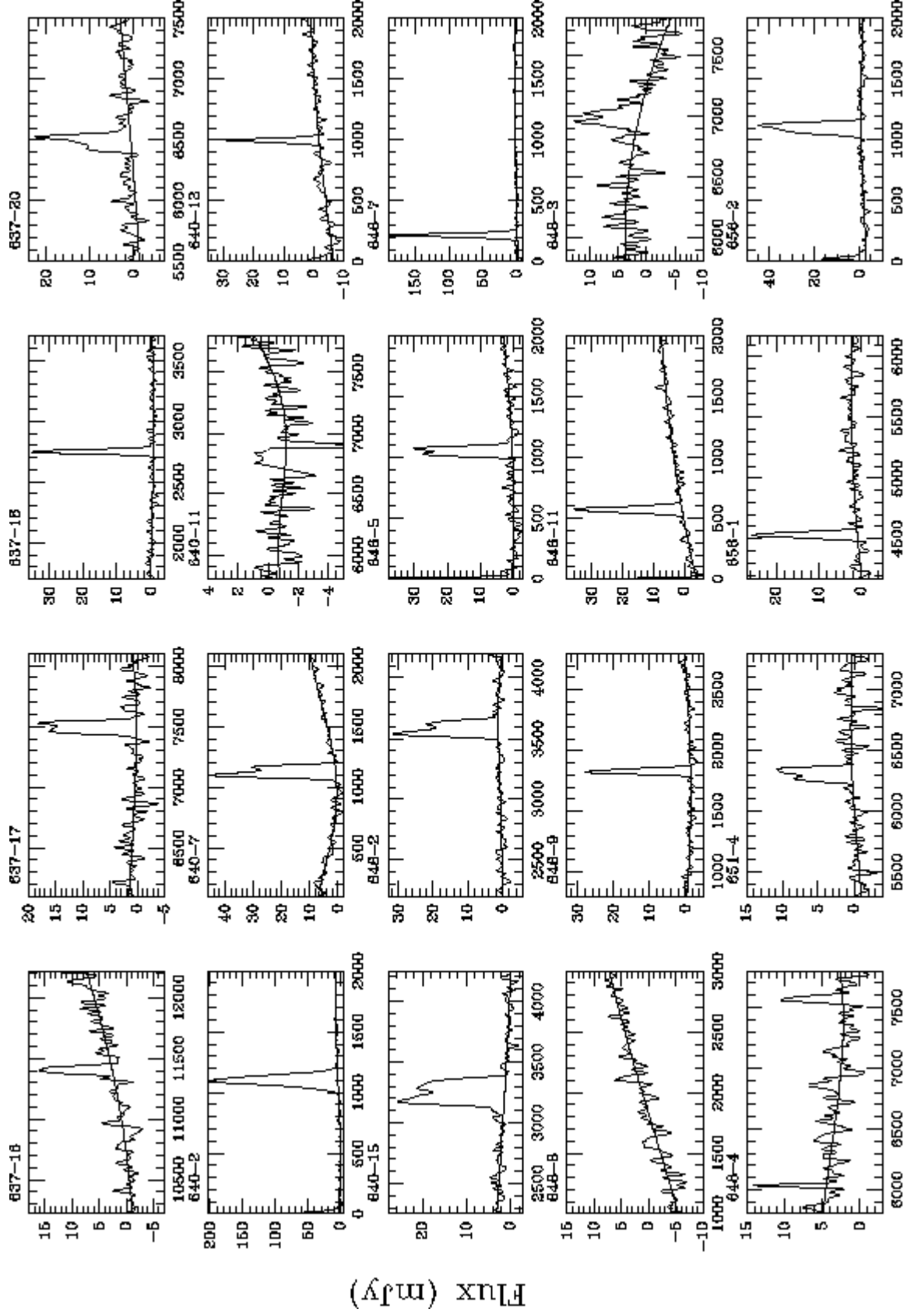




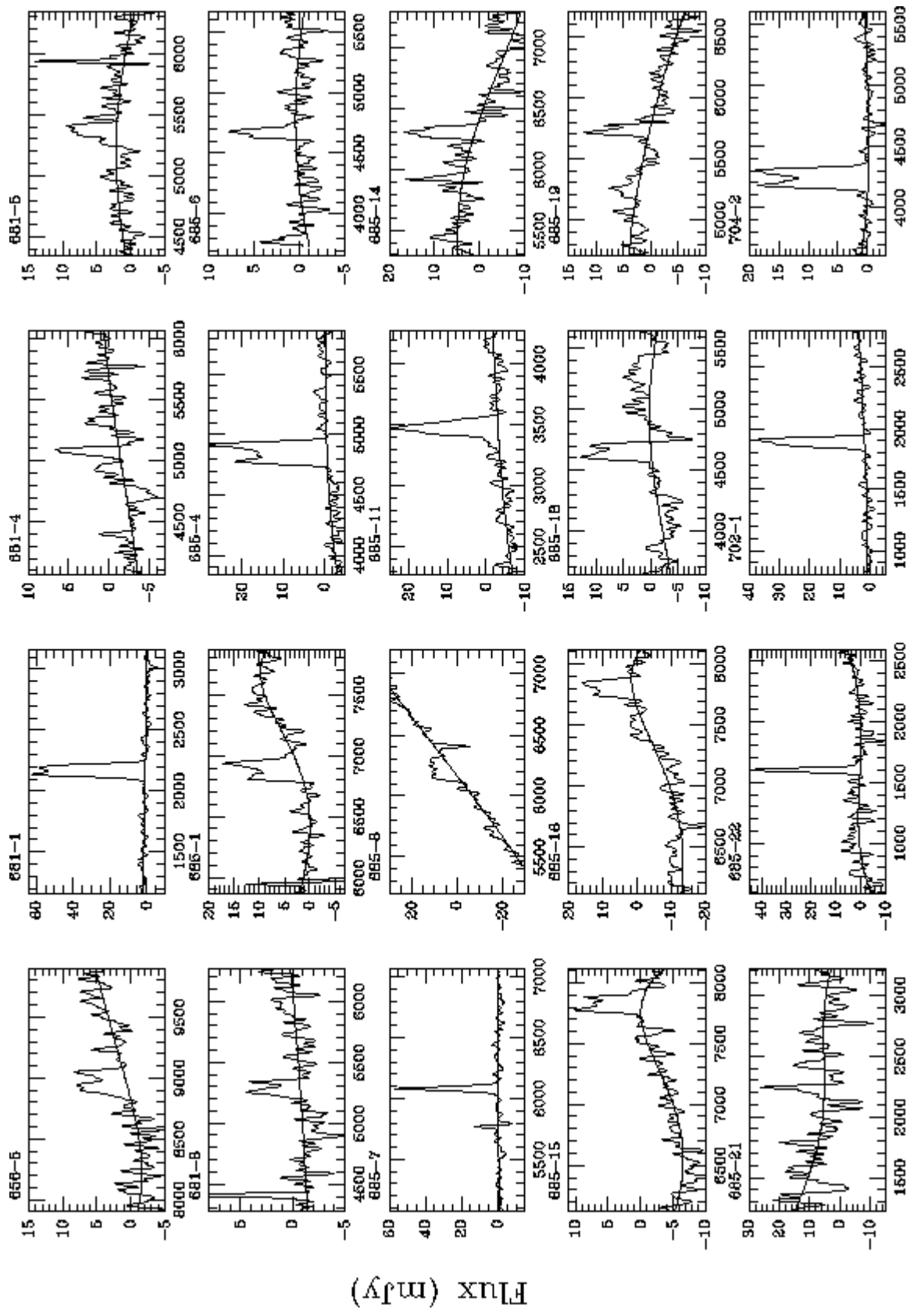
Velocity (km/sec)

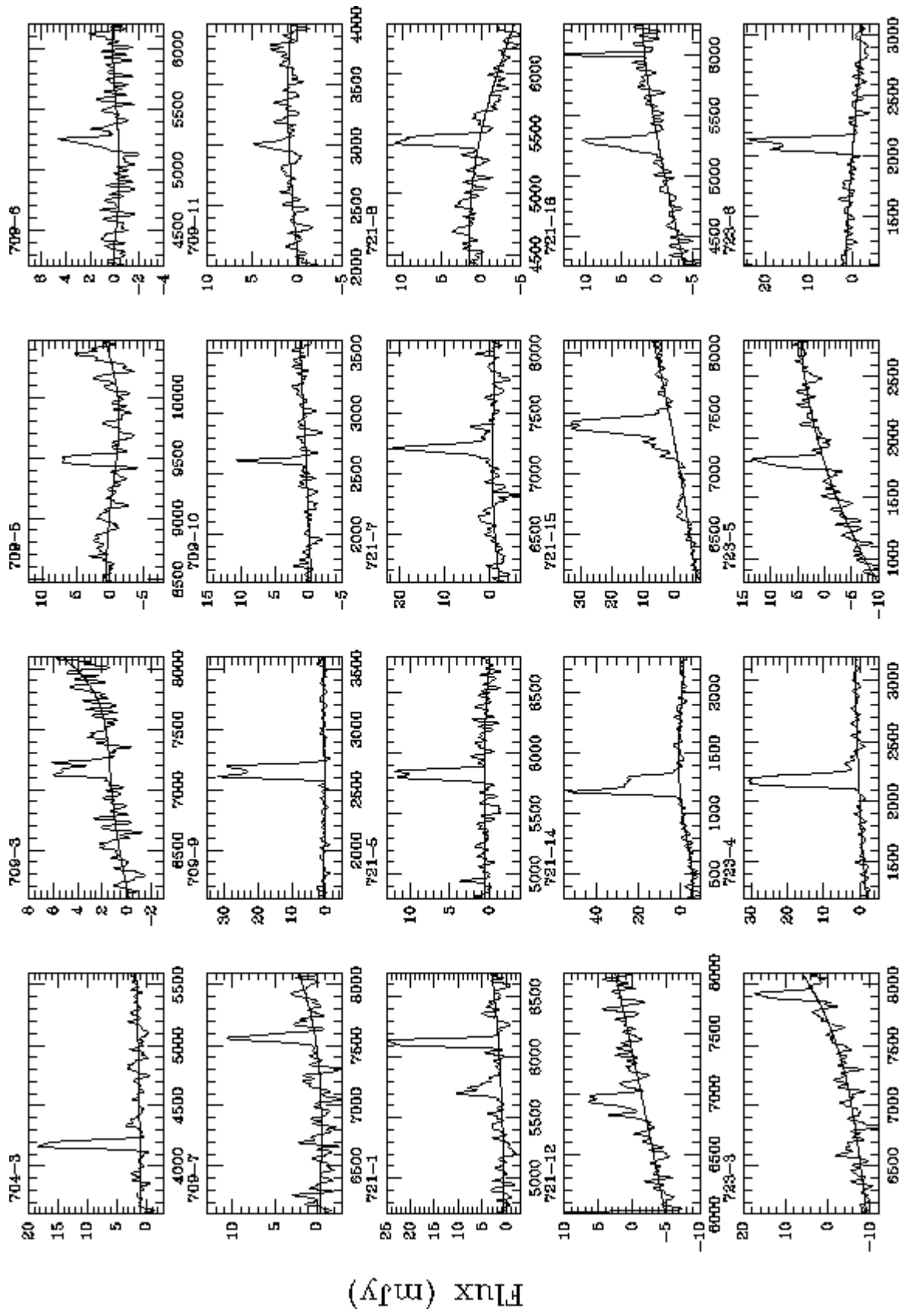


Velocity (km/sec)

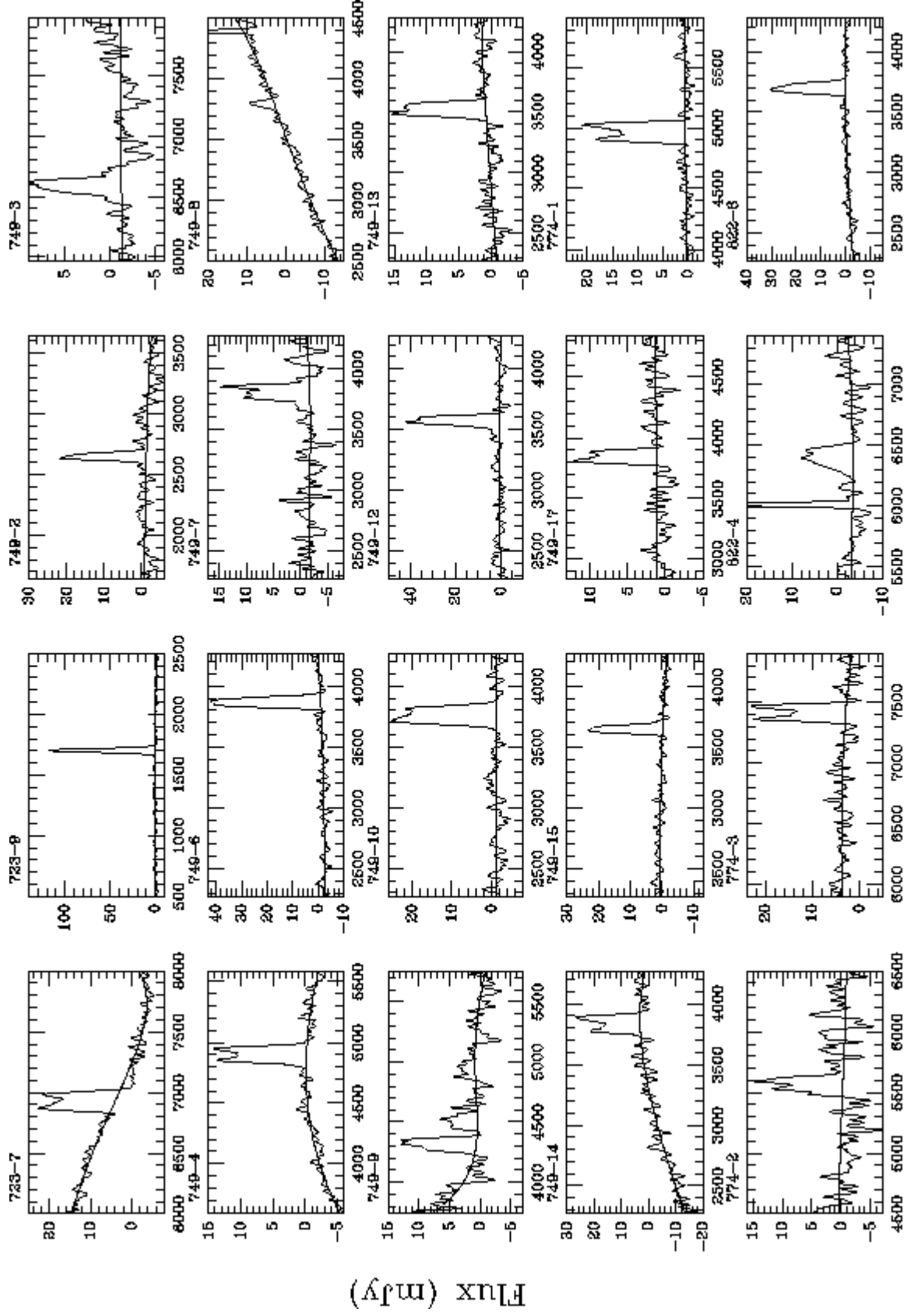


Velocity (km/sec)

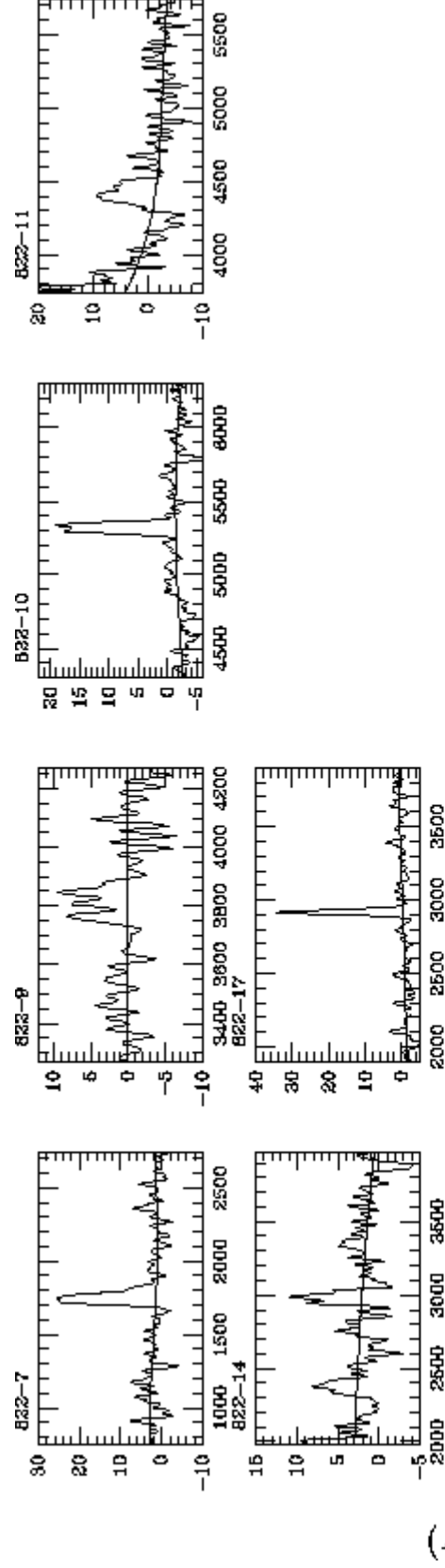




Velocity (km/sec)



Velocity (km/sec)



Velocity (km/sec)

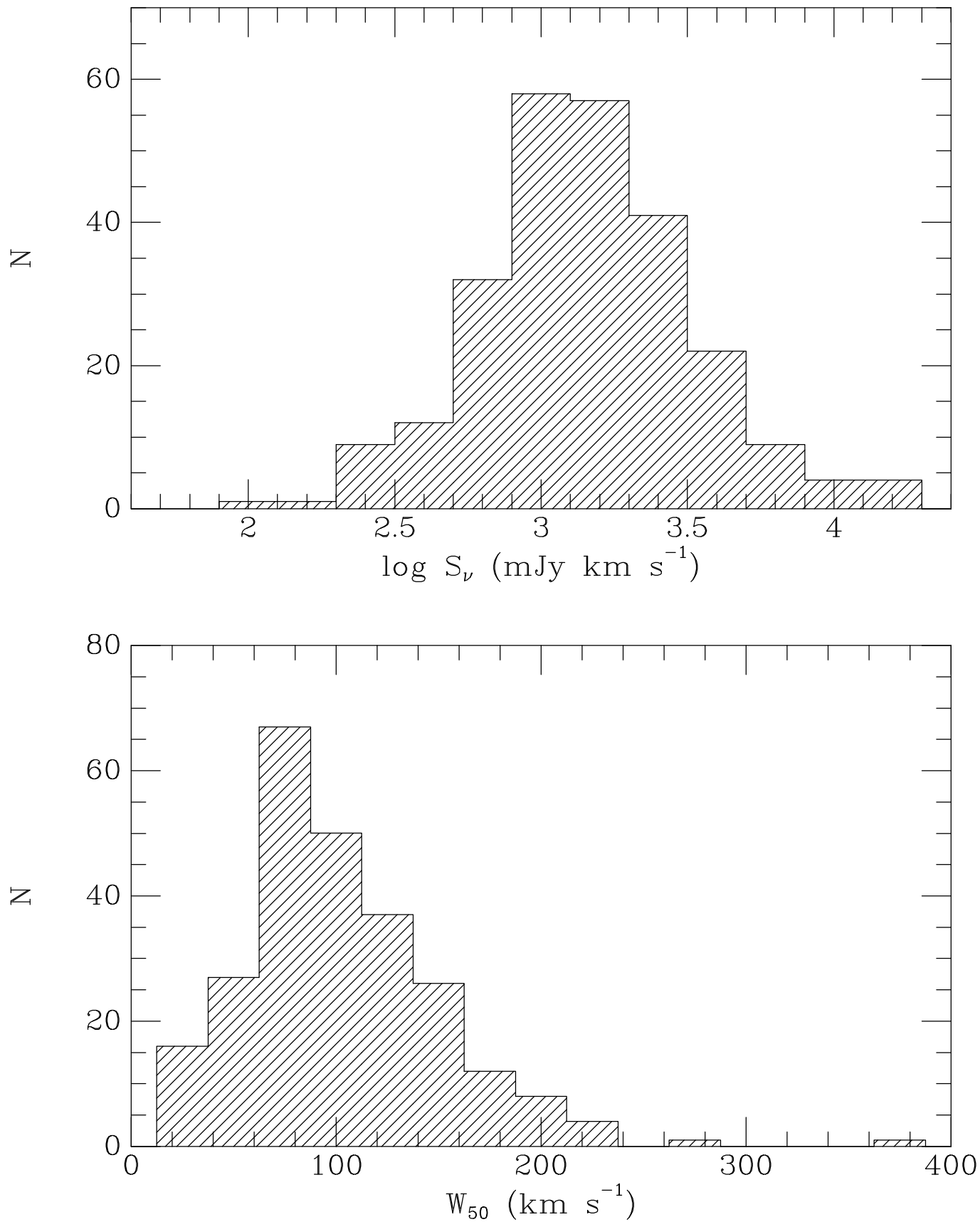


Figure 2

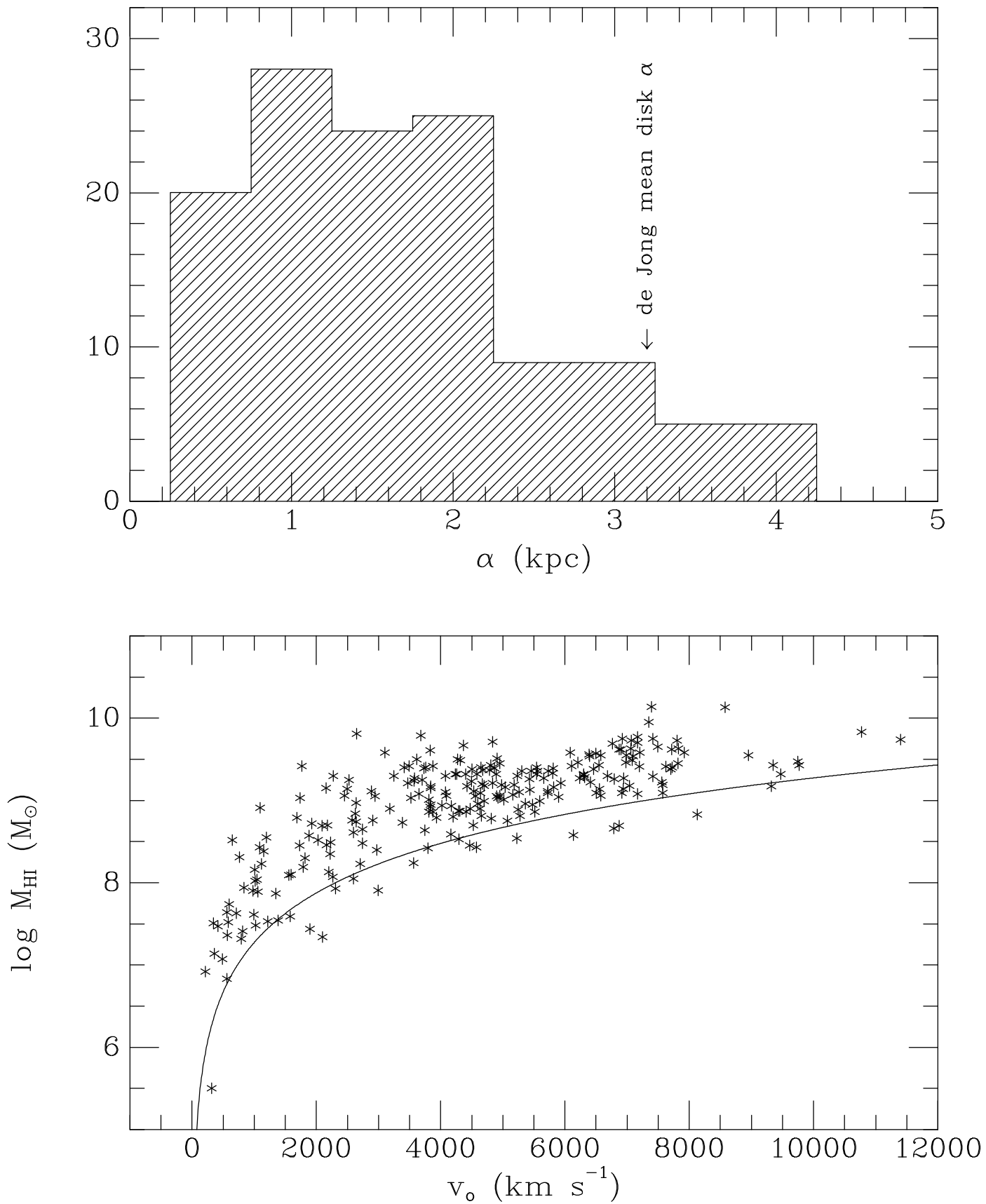


Figure 3

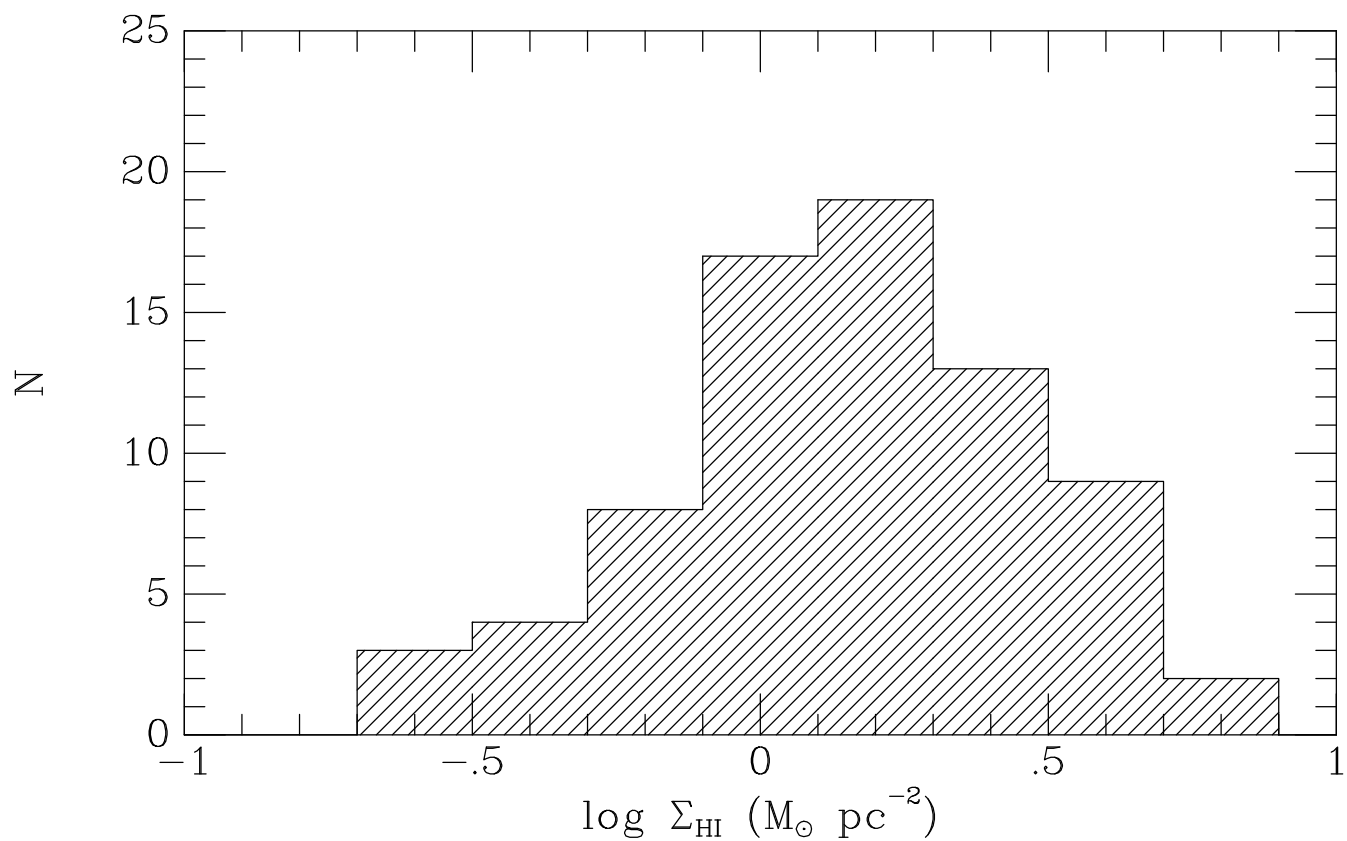
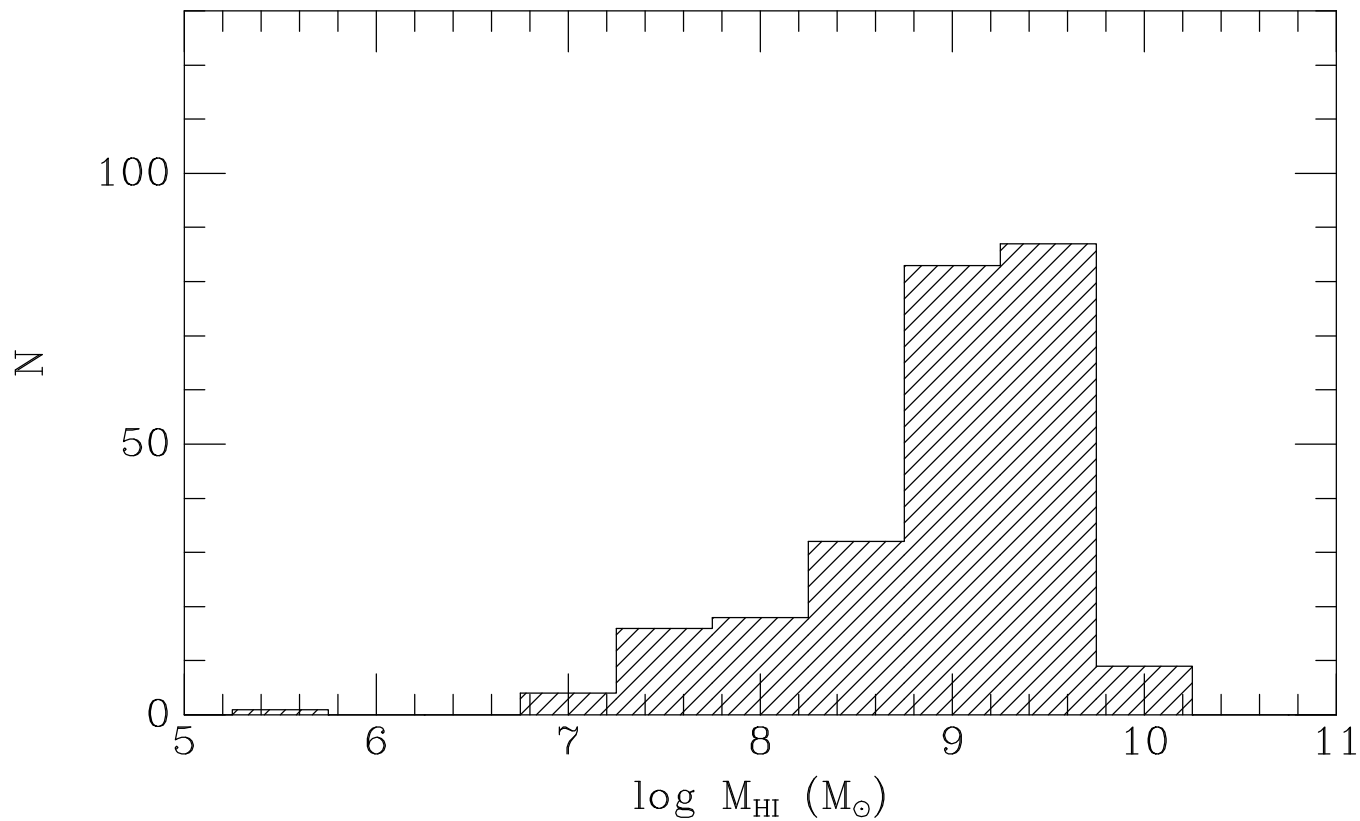


Figure 4

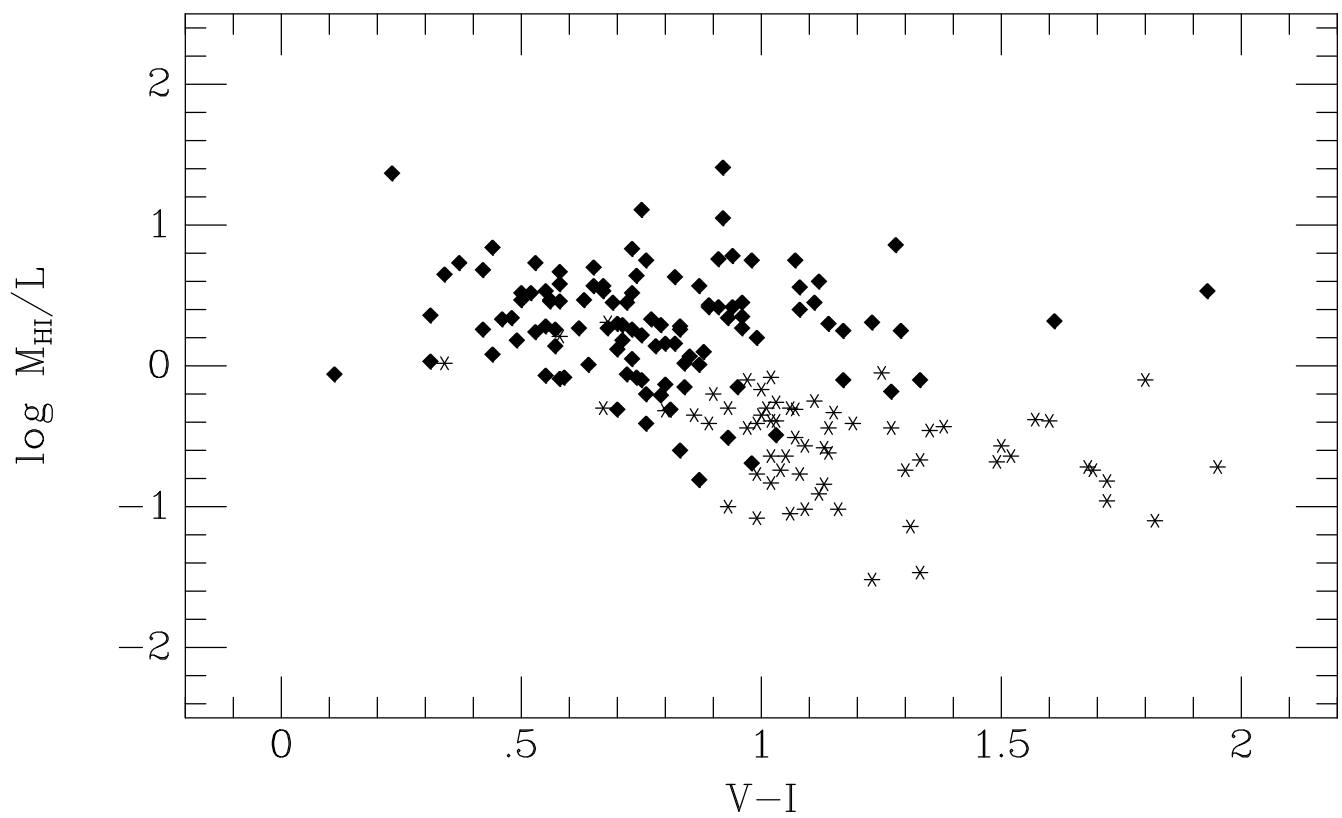
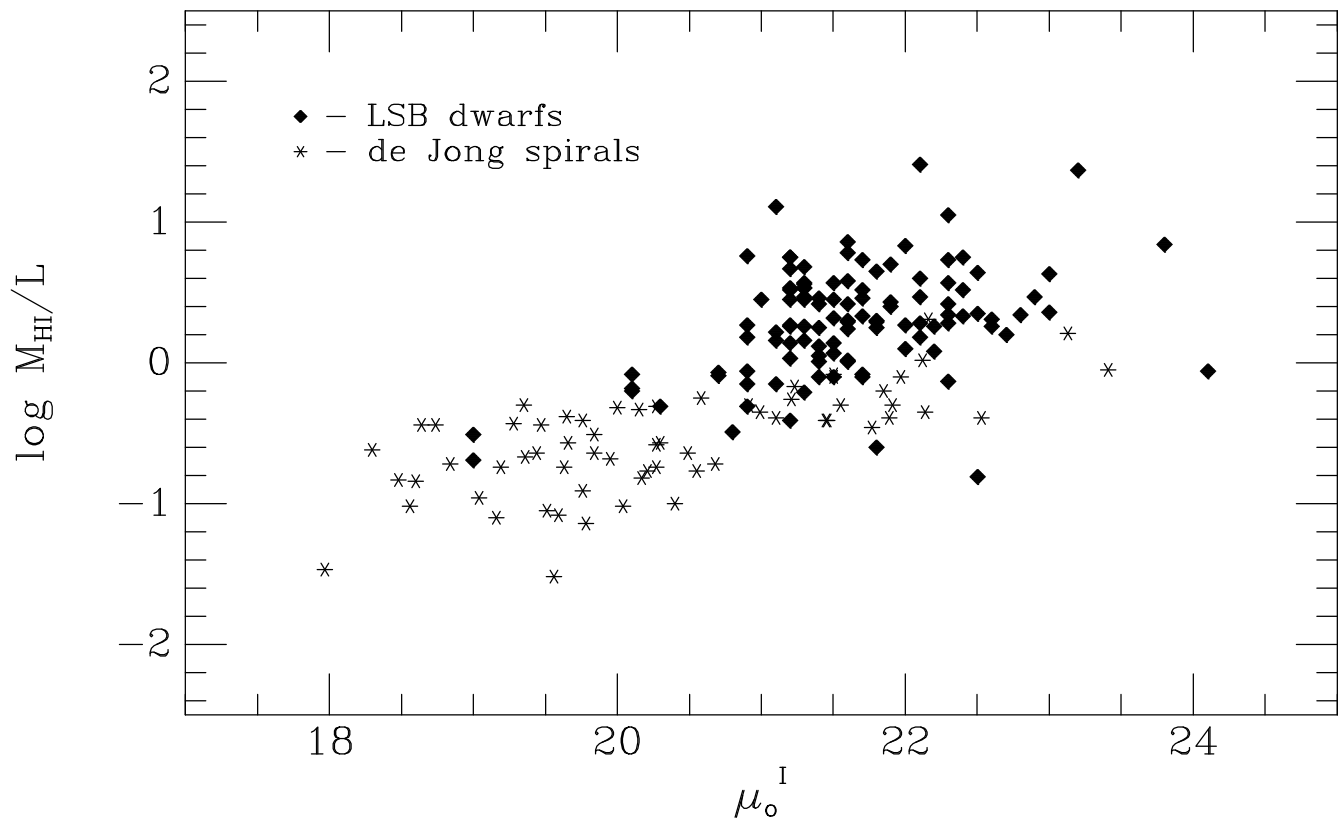


Figure 5

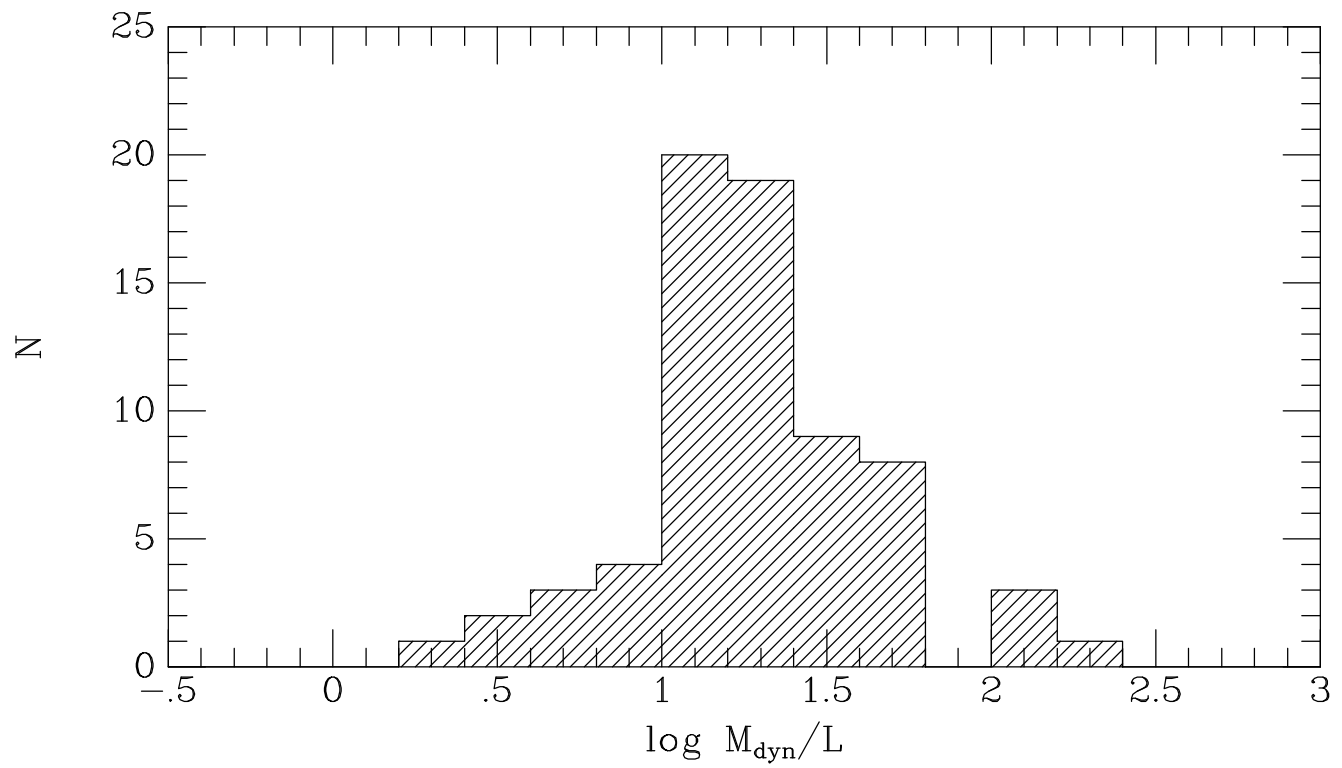
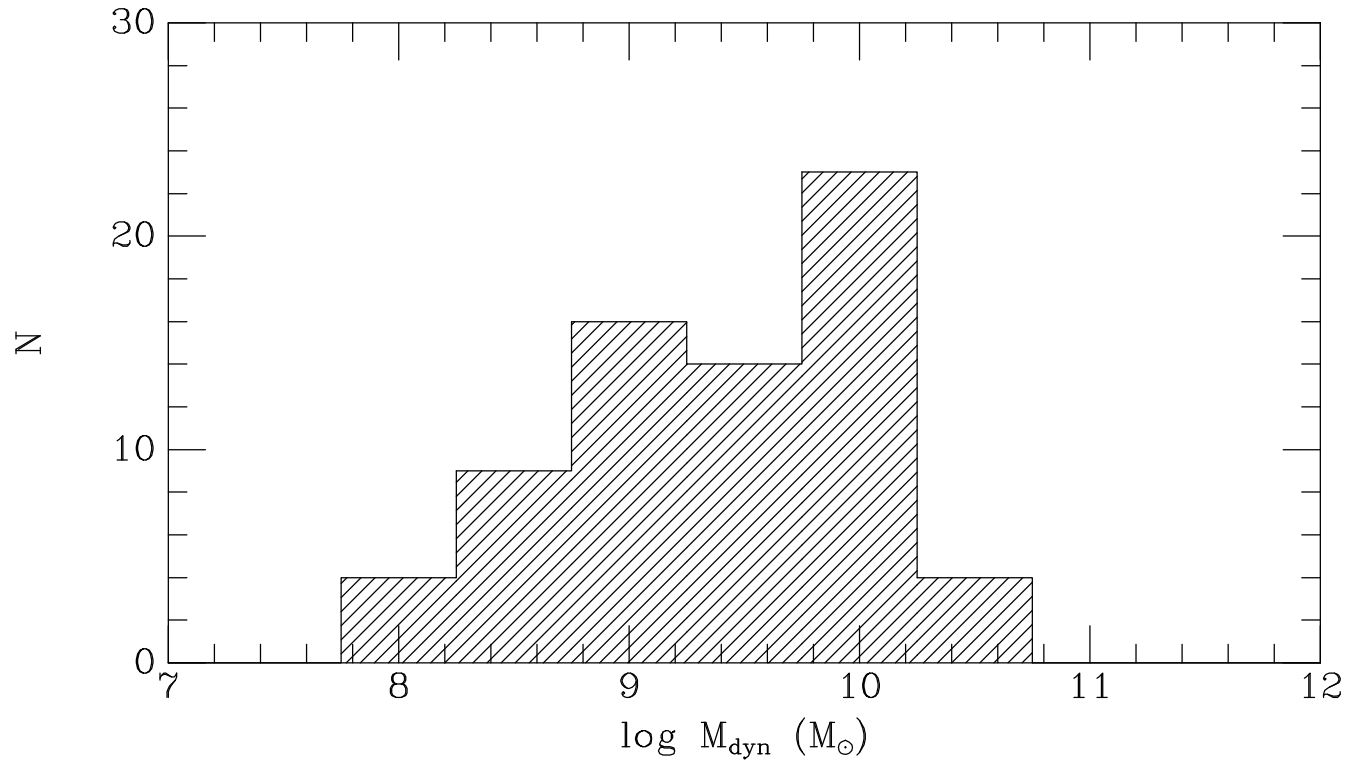


Figure 6

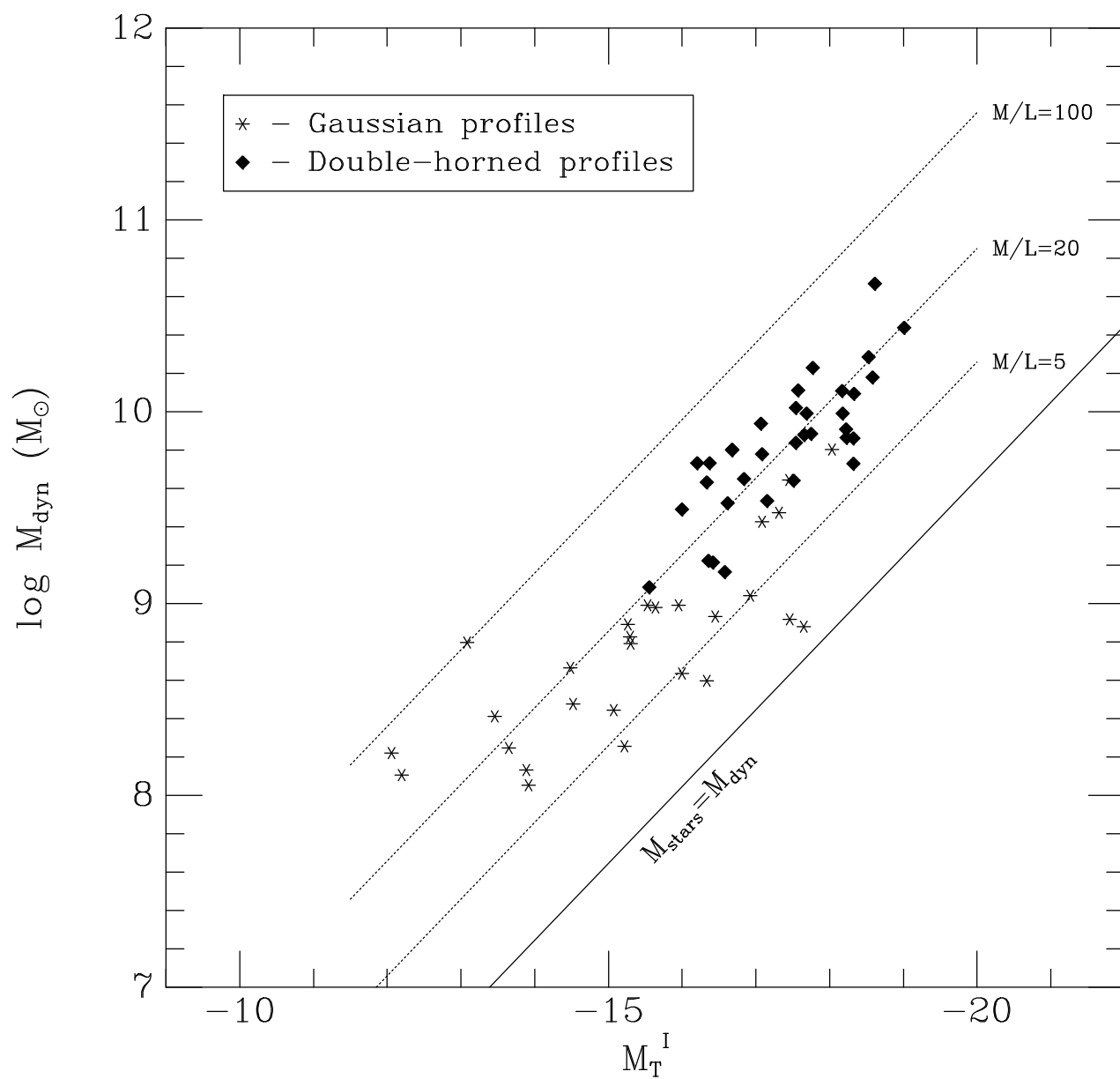


Figure 7

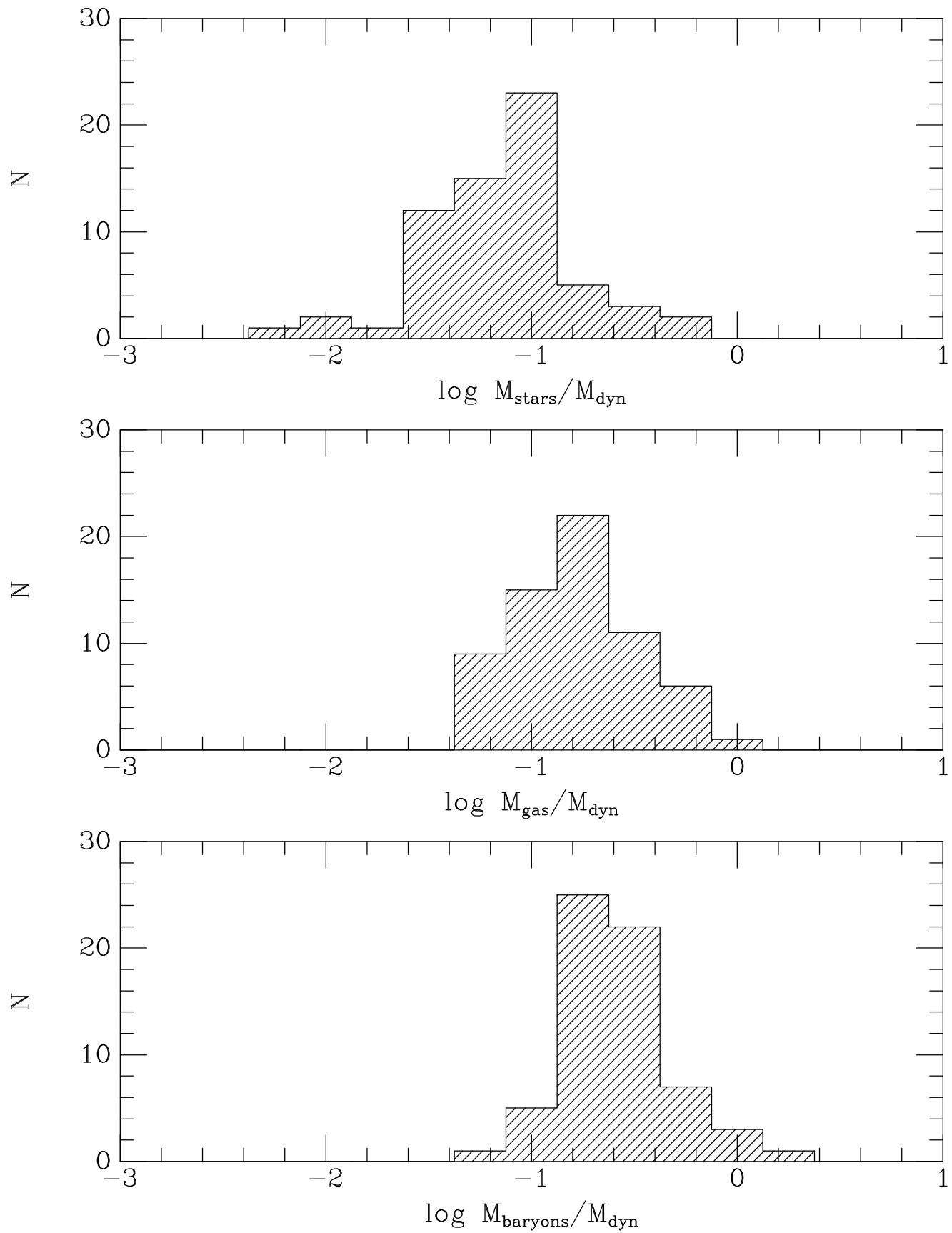


Figure 8